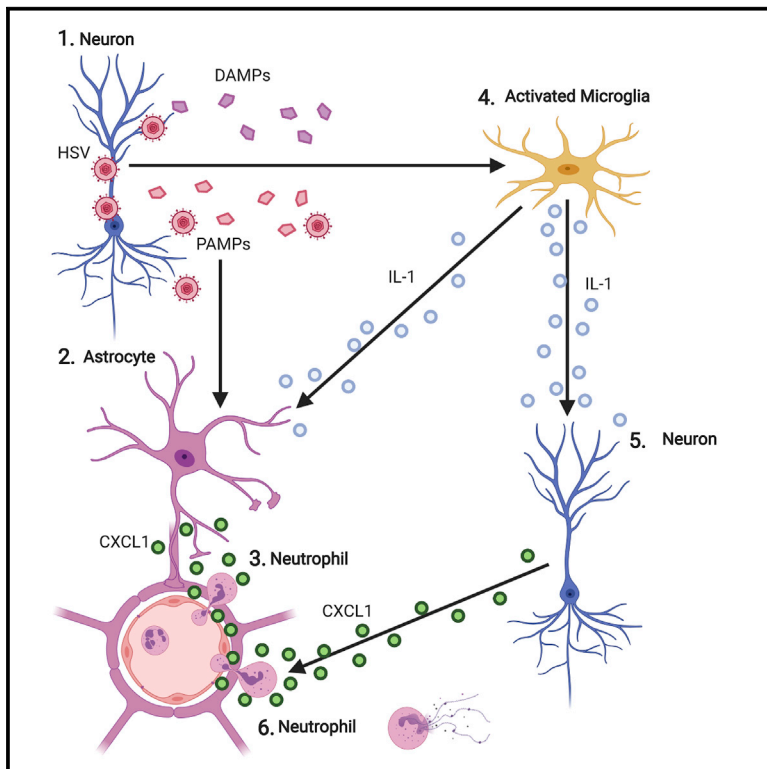**Article**

Astrocyte- and Neuron-Derived CXCL1 Drives Neutrophil Transmigration and Blood-Brain Barrier Permeability in Viral Encephalitis

Graphical Abstract

Authors

Benedict D. Michael,
Laura Bricio-Moreno,
Elizabeth W. Sorensen, ..., Tom Solomon,
Evelyn A. Kurt-Jones, Andrew D. Luster

Correspondence

aluster@mgh.harvard.edu

In Brief

Viral encephalitis results in brain injury despite effective anti-viral therapy. Michael et al. find that neutrophil entry into the brain drives morbidity in a mouse model of HSV-1 encephalitis. Neutrophil recruitment required CXCR2 and its ligand CXCL1, which represent attractive therapeutic targets to limit brain injury associated with encephalitis.

Highlights

- CXCR2 controls neutrophil recruitment into the brain in HSV-1 encephalitis

- $Cxcr2^{-/-}$ mice have decreased BBB permeability and improved outcome in HSV-1 infection

- CXCL1 is produced by both astrocytes and neurons in response to IL-1α

- CXCL1-CXCR2 is required for neutrophil transendothelial migration into the brain

CellPress

Article

Astrocyte- and Neuron-Derived CXCL1 Drives Neutrophil Transmigration and Blood-Brain Barrier Permeability in Viral Encephalitis

Benedict D. Michael,[1,2,3,6] Laura Bricio-Moreno,[1,6] Elizabeth W. Sorensen,[1] Yoshishige Miyabe,[4] Jeffrey Lian,[1] Tom Solomon,[2,3] Evelyn A. Kurt-Jones,[5] and Andrew D. Luster[1,7,*]

[1]Center for Immunology and Inflammatory Diseases, Division of Rheumatology, Allergy, and Immunology, Massachusetts General Hospital and Harvard Medical School, Boston, MA 02114, USA
[2]National Institute for Health Research, Health Protection Research Unit in Emerging and Zoonotic Infections, Institute of Infection, Veterinary and Ecological Sciences, University of Liverpool, Liverpool, L69 7BE, UK
[3]The Walton Centre NHS Foundation Trust, Department of Neurology, Liverpool L9 7LJ, UK
[4]Department of Cell Biology, Institute for Advanced Medical Sciences, Nippon Medical School, Tokyo 113-8602, Japan
[5]University of Massachusetts Medical School, Department of Medicine, Division of Infectious Disease and Immunology, Worcester, MA 01655, USA
[6]These authors contributed equally
[7]Lead Contact
*Correspondence: aluster@mgh.harvard.edu
https://doi.org/10.1016/j.celrep.2020.108150

SUMMARY

Herpes simplex virus (HSV)-1 encephalitis has significant morbidity partly because of an over-exuberant immune response characterized by leukocyte infiltration into the brain and increased blood-brain barrier (BBB) permeability. Determining the role of specific leukocyte subsets and the factors that mediate their recruitment into the brain is critical to developing targeted immune therapies. In a murine model, we find that the chemokines CXCL1 and CCL2 are induced in the brain following HSV-1 infection. *Ccr2* (CCL2 receptor)-deficient mice have reduced monocyte recruitment, uncontrolled viral replication, and increased morbidity. Contrastingly, *Cxcr2* (CXCL1 receptor)-deficient mice exhibit markedly reduced neutrophil recruitment, BBB permeability, and morbidity, without influencing viral load. CXCL1 is produced by astrocytes in response to HSV-1 and by astrocytes and neurons in response to IL-1α, and it is the critical ligand required for neutrophil transendothelial migration, which correlates with BBB breakdown. Thus, the CXCL1-CXCR2 axis represents an attractive therapeutic target to limit neutrophil-mediated morbidity in HSV-1 encephalitis.

INTRODUCTION

Viral encephalitis, which most commonly results from herpes simplex virus type 1 (HSV-1), is characterized by the early migration of neutrophils and monocytes into the brain, forming perivascular cuffs and increased blood-brain barrier (BBB) permeability (Masanti and Weller, 2004). Despite treatment with the nucleoside analog acyclovir, there is marked cerebral edema; furthermore, 10%–20% of patients die, and most survivors have significant neurological sequelae (Venkatesan et al., 2019). Biomarkers of BBB permeability and cerebral edema, visualized by brain imaging, correlate with a poor outcome and with inflammatory cytokines and chemokines relating to interleukin (IL)-1α and IL-1β in the cerebrospinal fluid (CSF) of patients with viral encephalitis (Michael et al., 2016b). Elevated levels of myeloperoxidase, reflecting neutrophil numbers and degranulation, are also found in the CSF (Michael et al., 2016a), and prolonged detection of neutrophils in the CSF correlates with CSF CXCL1 concentration and neurological sequelae (Grygorczuk et al., 2018). In murine models, intracranial (i.c.) injection of IL-1β is associated with neutrophil migra-

tion into the brain and impairment of BBB integrity, although the exact underlying mechanisms remain to be elucidated (Bolton et al., 1998). In particular, the predominant neuroglia responsible for production of the principal cytokines and chemokines that leads to neutrophil recruitment, retention as perivascular cuffs, and consequent breakdown of the BBB are poorly understood.

In an attempt to reduce cerebral edema, corticosteroids are sometimes given. However, because of their broad immunosuppressive effects, there is concern that this may license increased viral replication, and it is unclear whether on balance they are beneficial (Meyding-Lamadé et al., 2003; Solomon et al., 2012). An improved understanding of the biological mechanisms driving the migration of specific leukocyte populations into the brain and breakdown of the BBB are required to develop targeted immunotherapies to reduce the transmigration of precise deleterious leukocyte populations and maintain the integrity of the BBB without risking uncontrolled viral replication (Venkatesan et al., 2019).

Intravital microscopy studies of i.c. infection with HSV-1 demonstrate increased leukocyte rolling and adhesion in association with upregulation of multiple chemokines, but the

differential role of specific leukocyte subsets, their corresponding chemokine receptor-ligand interactions, and the pivotal stages of transmigration affecting on BBB permeability have not been elucidated (Vilela et al., 2008). It has been found that i.c. infection with the non-cytopathic lymphocytic choriomeningitis virus (LCMV) is associated with marked myeloid cell infiltration and breakdown of the BBB (Kim et al., 2009). In this model, abrogation of monocyte recruitment using $Ccr2^{-/-}$ mice does not alter mortality. However, depletion of both monocytes and neutrophils using a combination of $Ccr2^{-/-}$ mice treated with αGr1 antibody results in reduced mortality (Kim et al., 2009). Similarly reduced hippocampal injury in response to picornavirus infection has been reported following inhibition of monocyte and neutrophil recruitment (Howe et al., 2012). Conversely, i.c. infection with HSV-1, which is cytopathic, is associated with increased mortality when animals are deficient in monocyte cell recruitment, i.e., when using an αCCL2 antibody or $Ccr2^{-/-}$ mice (Boivin et al., 2012; Conrady et al., 2013; Menasria et al., 2016). This discrepancy in the role of myeloid cell infiltration in different brain infections warrants further investigation so that directed treatment can be developed. In addition, although the role of chemokines in modulating intravascular leukocyte dynamics is frequently studied, the role of these ligands following transendothelial migration is less well understood (Kim et al., 2009; Teixeira et al., 2010; Vilela et al., 2010, 2013). Even though astrocytes are recognized to play a pivotal role in the maintenance of tight junctions and adherens junctions of cerebral capillaries and post-capillary venules that form the BBB, their role in inducing leukocyte migration and BBB permeability in viral encephalitis have not been fully elucidated (Klein and Hunter, 2017).

We report that chemokine expression and leukocyte migration into the brain continued beyond the immediate clearance of replicating HSV-1 with acyclovir treatment, with sustained expression of the chemokines CCL2 and CXCL1 and ongoing migration of inflammatory monocytes and neutrophils. Attenuation of CCL2 signaling using $Ccr2^{-/-}$ mice resulted in decreased monocyte recruitment, uncontrolled viral replication, BBB breakdown, and increased morbidity. Conversely, abrogation of CXCL1 signaling in $Cxcr2^{-/-}$ mice was associated with marked reduction in both neutrophil recruitment and BBB permeability, along with reduced morbidity, without substantively altering viral control. Using a combination of confocal microscopy and *in vitro* studies, we demonstrate that CXCL1 is expressed by perivascular astrocytes in response to HSV-1 infection and by both astrocytes and neurons in response to IL-1α. Using intravital microscopy, we demonstrate that CXCR2 is required for both neutrophil transmigration and retention in the abluminal perivascular space and that extravasated neutrophils promote subsequent increased BBB permeability. Notably, although antibody blockade of CXCL1 exerted a lesser effect on neutrophil arrest than $Cxcr2$ deficiency, the αCXCL1 antibody was as effective at inhibiting neutrophil transendothelial migration and abluminal accumulation as $Cxcr2$ deficiency. These studies identify the CXCL1-CXCR2 axis as a key promoter of increased BBB permeability in HSV-1 encephalitis. Altogether, these findings suggest that adjunctive immunomodulatory therapy, particularly targeting CXCL1 and neutrophil transendothelial migration, may improve outcomes in HSV-1 encephalitis and could have broader implications for viral encephalitis.

RESULTS

HSV-1 Infection Leads to Increased BBB Permeability, Leukocyte Infiltration, and Morbidity despite Acyclovir

To examine the dissemination of HSV-1 infection in the parenchyma following i.c. infection, C57BL/6 mice were anaesthetized with isoflurane. A sterile Teflon depth-restricted needle was used to perform i.c. inoculation with 1×10^5 PFU/mouse or sham infection with sterile PBS into the subarachnoid space. At day post-infection (DPI) 1, mice were euthanized and whole-brain tissue was fixed, frozen, and analyzed by confocal microscopy. Although HSV-1-infected neuroglia could be identified throughout the cerebral tissue, there was a predilection for the hippocampus, which is reflective of human disease (Figure 1A) (Barnett et al., 1994). To confirm these findings, we repeated the inoculation procedure with VP26-EGFP-expressing HSV-1 and again identified that the principal region of virus infection (marked by viral fluorescence) was the hippocampus (Figure 1B). To assess the impact of infection on BBB permeability, C57BL/6 mice received HSV-1 or sterile PBS i.c. as earlier, and then on DPI 1, mice received an intravenous (i.v.) injection of Evans blue dye and 30 min later were sacrificed and perfused to clear intravascular dye. The appearance of Evans blue in the brain parenchyma and meninges was assessed as a measure of BBB permeability. Representative whole brains demonstrated marked extravasation of Evans blue dye following HSV-1 infection, reflecting increased BBB permeability (Figure 1C). To confirm these findings, HSV-1- or sham-infected mice received an i.v. injection of fluorescein isothiocyanate (FITC)-labeled albumin on DPI 1. After 1 h, whole-brain tissue was obtained and prepared for confocal microscopy. In sham-infected brain, little extravasated albumin was seen; however, in response to HSV-1 infection, there was a significant extravasation of albumin into the brain parenchyma, around both meninges, and into the cerebral vasculature (Figures 1D and 1E). Thus, both Evans blue dye and labeled albumin studies demonstrated increased BBB permeability following HSV-1 infection.

To determine the impact of antiviral treatment on encephalitis, sham- and HSV-1-infected mice received a daily dose of either acyclovir or sterile PBS intraperitoneally (i.p.) starting 24 h post-infection. In this model of acute, severe HSV-1 encephalitis, there was no significant difference in either morbidity or mortality following infection between the acyclovir-treated and the untreated groups (Figure 1F) despite expedited clearance of replicating HSV-1 by DPI 3 with acyclovir treatment (Figure 1G). Remarkably, the influx of both neutrophils (CD45^{hi}/CD11b$^+$/Ly6-G^{hi}/Ly6C^{int}) and inflammatory monocytes (CD11b$^+$/CD45^{hi}/Ly6C$^+$/Ly6G$^-$) was observed despite acyclovir treatment and viral clearance (Figure 1H). Although neutrophil migration was noted as soon as 6 h post-infection, inflammatory monocytes did not increase until 24 h post-infection (Figures 1I and 1J); however, both neutrophil and inflammatory monocyte levels remained consistently elevated at DPI 5 with and without acyclovir-dependent viral clearance. Flow cytometry of whole brain was also performed with conjugated antibodies to CD3, CD4, CD8, and natural killer cells in initial experiments, but because of the marked predominance of neutrophils and monocytes at these time points, these cell types were not evaluated further (data not shown).
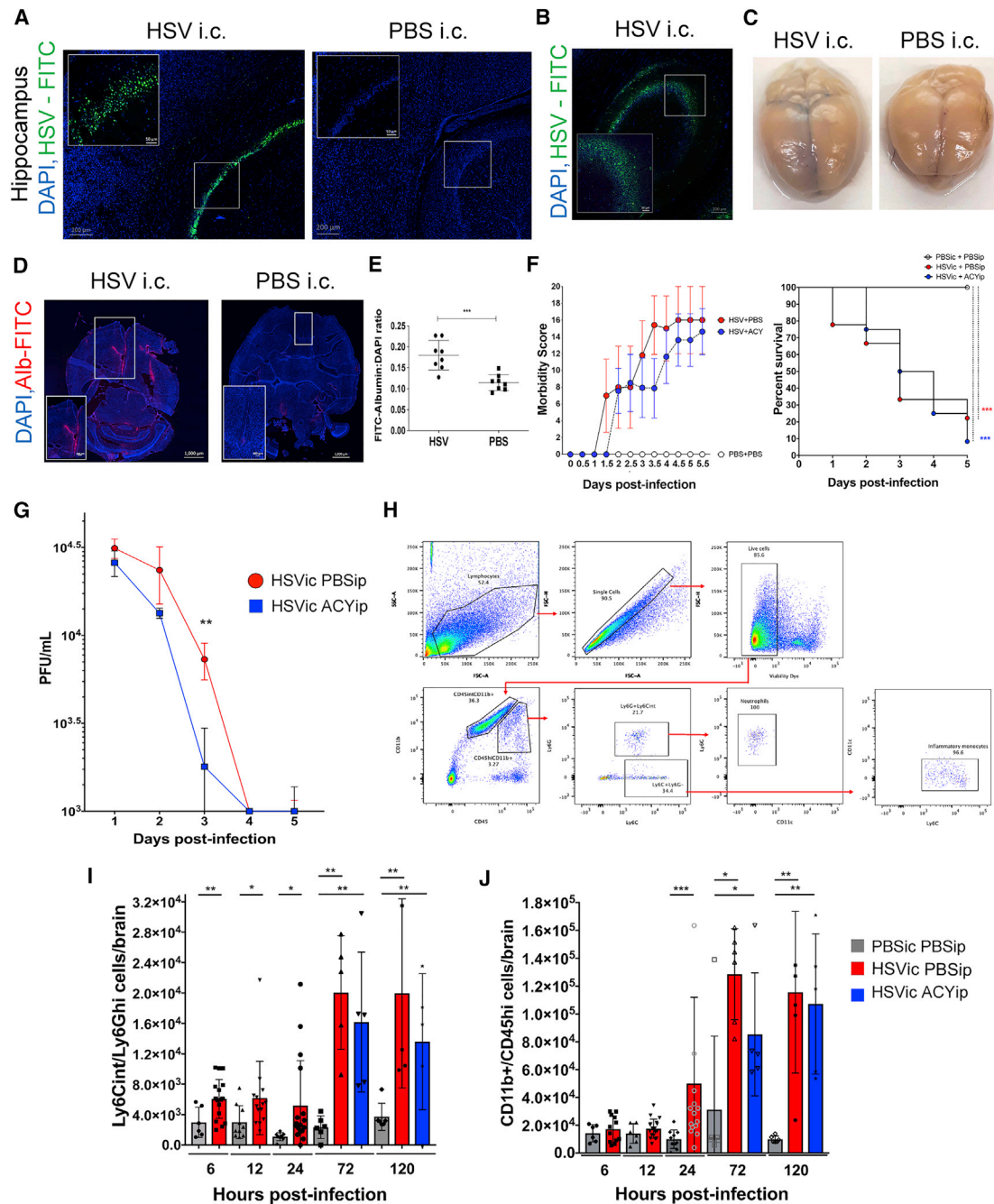
Figure 1. HSV-1 Infection Leads to Increased BBB Permeability, Leukocyte Transmigration, and Morbidity Despite Acyclovir

(A) Immunohistochemistry was performed on axial sections of brain tissue following i.c. infection with HSV-1 (HSV i.c.) or sham infection with sterile PBS (PBS i.c.) on DPI 1 (n = 3/group, scale bars: 50 and 200 μm).

(B) Confocal microscopy was performed on axial sections of brain tissue following i.c. HSV-EGFP injection on DPI 1 (n = 3/group, scale bars: 50 and 200 μm).

(C) 24 h following i.c. HSV-1 or sterile PBS injection, mice received Evans blue i.v. 30 min before euthanasia and craniotomy (n = 5/group).

(D and E) 24 h following i.c. HSV or sterile PBS injection, mice received FITC-albumin i.v. 1 h before euthanasia. (D) Immunohistochemistry was performed on axial sections (n = 4/group, scale bars: 100, 200, and 1,000 μm), and (E) FITC-albumin quantitated and presented as mean ± SD (n = 8/group).

(F) Morbidity score and mortality were determined every 12 h following i.c. infection with HSV-1 using an established scoring system presented as mean ± SEM (n = 10/group).

(G) Viral load was determined by plaque assay of whole-brain homogenate (n = 11/group).

(H–J) Gating strategy (H) for flow cytometric analysis of neutrophils and monocytes recovered from whole brains 6–120 h following infection to quantify neutrophil (Ly6Ghi/Ly6Cint) (I) and inflammatory monocyte (CD11b+/CD45hi) (J) recruitment (n = 6–18/group). Data are presented mean ± SD.

*p < 0.05; **p < 0.01; ***p < 0.001.

Cxcr2 Deficiency Reduces Neutrophil Recruitment, BBB Permeability, and Morbidity

We next examined the production of chemokines and associated cytokines during the course of infection to assess potential mediators that might promote migration of these leukocyte populations. HSV-1- or sham-infected mice again received a daily dose of either acyclovir or PBS i.p. starting at 24 h post-infection and were euthanized during the early (DPI 1–3) or late (DPI 4–5) time points. Whole-brain homogenate was analyzed by Luminex multiplex assay. Despite acyclovir, significant upregulation of many CC and CXC chemokines was identified at both early and late time points, particularly CCL2 and CXCL1, along with IL-1α (Figures 2A and S1). Chemokine and cytokine levels remained elevated despite acyclovir treatment, suggesting that marked viral replication was not necessary for sustained chemokine expression following HSV-1 infection of the brain.

To determine the impact of specific chemokine signaling pathways on HSV-1 infection and brain inflammation, mice lacking the cognate receptors for these ligands were studied. First, $Ccr2^{-/-}$ and $Cxcr2^{-/-}$ mice were infected i.c. with HSV-1 and morbidity and mortality were assessed. $Ccr2^{-/-}$ mice, which lack the receptor for CCL2, had a significant increase in morbidity scores (Figure 2B). In contrast, $Cxcr2^{-/-}$ mice, which lack the receptor for CXCL1, had a less morbid phenotype, which was particularly evident when morbidity scores were expressed relative to those of wild-type (WT) mice despite acyclovir treatment of all groups (Figure 2C). $Cxcr2^{-/-}$ mice also had a trend toward reduced mortality, although $Ccr2^{-/-}$ mice showed no significant differences in mortality when compared with WT mice (Figure 2D).

To determine the impact of abrogation of signaling through these two chemokine receptors on leukocyte migration, we studied neutrophils and inflammatory monocytes in $Cxcr2^{-/-}$ and $Ccr2^{-/-}$ mice infected with HSV-1. On DPI 1, whole-brain tissue was prepared for flow cytometry immediately post-mortem following intracardiac perfusion to minimize intravascular cell collection. As anticipated, $Cxcr2^{-/-}$ mice had a marked reduction in neutrophil (CD45hi/CD11b+/Ly6Ghi/Ly6Cint) infiltration yet retained inflammatory monocyte (CD11b+/CD45hi/Ly6C+/Ly6G−) infiltration (Figure 2E). Conversely, $Ccr2^{-/-}$ mice had a marked reduction in inflammatory monocyte infiltration with ongoing neutrophil recruitment. Whereas there was no difference in viral load at DPI 3 between WT and $Cxcr2^{-/-}$ mice, $Ccr2^{-/-}$ mice had a dramatic increase in viral load (Figure 2F). These results suggested that neutrophil infiltration is detrimental during HSV-1 encephalitis.

To assess the spatial distribution of neutrophils in the HSV-1-infected brain relative to the resident myeloid-lineage cells, microglia, we infected CCR2-RFP/CX3CR1-GFP reporter mice (Saederup et al., 2010) i.c. with HSV-1, and on DPI 1, cerebral cortex was obtained for whole-mount microscopy. *Ex vivo* sections of the frontoparietal cortex were stained with an Ly6G antibody, and we observed that neutrophils (Ly6G+) predominated in perivascular albuminal spaces, whereas CCR2+ cells were not seen in the parenchyma in these sections (Figure 2G). Moreover, to confirm the detrimental effect of neutrophils during HSV-1 encephalitis, we used an anti-Ly6G antibody to deplete neutrophils

on DPI −1, 1, and 3. We observed that when neutrophils were depleted, there was a significant decrease in mortality and morbidity during HSV-1 encephalitis (Figure 2H). In addition, the ratio of the albumin concentration in the brain relative to the serum of infected mice was determined, reflecting BBB permeability, which demonstrated a marked reduction in BBB permeability in $Cxcr2^{-/-}$ mice relative to WT HSV-1-infected mice and, more significantly, to HSV-1-infected $Ccr2^{-/-}$ mice (Figure 2I). Altogether, these results demonstrated that CXCR2 is required for neutrophil migration and increased BBB permeability, which are associated with increased morbidity.

CXCL1 Is Produced by Astrocytes and Neurons

CXCL1 was the predominant CXCR2 ligand upregulated following HSV-1 infection (Figures 2A and S1). We also noted that IL-1α, a known activator of neutrophil migration, was upregulated following HSV-1 infection, as has been reported (Bolton et al., 1998). Therefore, we assessed the impact of the IL-1 receptor antagonist (IL-1RA) on CXCL1 production in the HSV-1-infected brain. IL-1RA treatment administered i.p. immediately following HSV-1 infection was compared with dexamethasone treatment, which has been previously reported to reduce delayed cerebral edema in a murine model of HSV-1 encephalitis (Meyding-Lamadé et al., 2003). Mice that received IL-1RA had a significant reduction in expression of CXCL1 during DPI 1–5 following i.c. HSV-1 infection, which was not seen with dexamethasone treatment (Figure 3A). We next examined which glial populations were associated with CXCL1 production. Following i.c. HSV-1 infection, whole-brain tissue was prepared on DPI 1 for confocal microscopy. Because astrocytes form an integral component of the BBB, and because HSV-1 infection is reported to induce robust expression of cytokines and chemokines by microglia (Marques et al., 2006), in addition to CXCL1, sections were stained for GFAP to mark astrocytes, CD11b to identify microglia, and NeuN to identify neurons, the primary locus of HSV-1 replication. CXCL1 expression did not co-localize with CD11b+ microglia but instead co-localized with perivascular GFAP+ astrocytes and NeuN+ neurons (Figures 3B–3D).

To confirm these observations, we assessed the expression of CXCL1 and 31 other inflammatory cytokines and chemokines in the supernatant of cultured primary neurons, microglia, and astrocytes following incubation with HSV-1 using the Luminex multiplex assay. There was marked induction of CXCL1 and CCL2 protein secretion by astrocytes following incubation with HSV-1 (Figure 3E). In addition, we evaluated the expression of IL-1α by neurons, microglia, and astrocytes and found that only microglia demonstrated induction of IL-1α when incubated with HSV-1 (Figure 3F). To determine whether CXCL1 production is the result of paracrine stimulation by IL-1α, we stimulated cultured primary neurons, microglia, and astrocytes with IL-1α (10 ng/mL) or control media *in vitro* and confirmed that both astrocytes and neurons, but not microglia, increase CXCL1 production after incubation with IL-1α (Figure 3G). This effect was abrogated by IL-1RA, confirming the results we observed *in vivo*. These data support the confocal microscopy data, which identified CXCL1 expression by neurons and astrocytes during HSV-1 encephalitis *in vivo*, whereas only astrocytes were demonstrated to produce CXCL1 *in vitro* in response to HSV-1 infection.
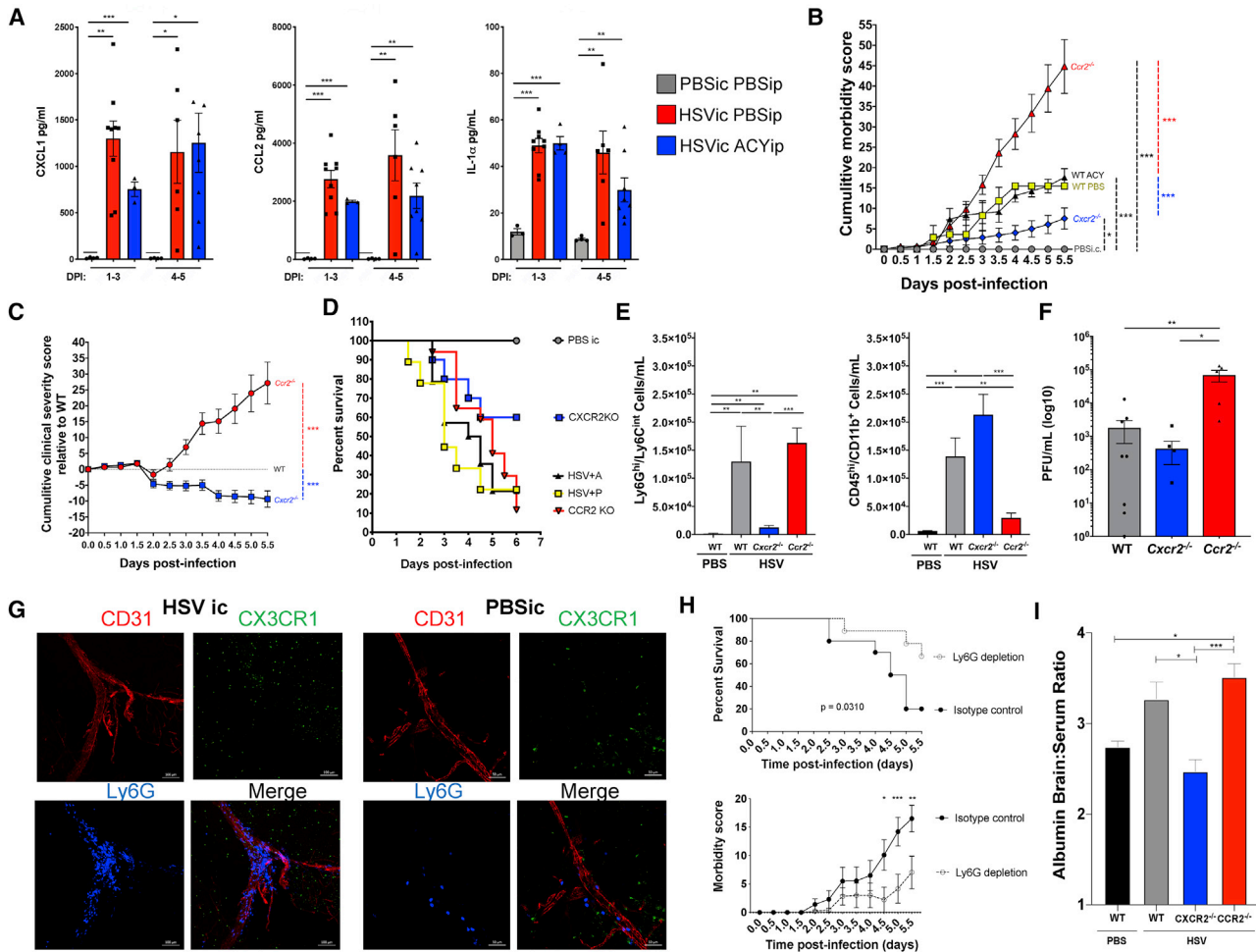
Figure 2. *Cxcr2* Deficiency Reduces Neutrophil Recruitment, BBB Permeability, and Morbidity

(A) Luminex multiplex protein assay was performed on whole-brain homogenate following i.c. HSV-1 or sterile PBS at early (DPI 1–3) and late (DPI 4–5) time points and presented as mean ± SEM (n = 4–12/group) in duplicate. See also Figure S1.

(B) Morbidity was determined every 12 h following HSV-1 infection of WT, *Ccr2*$^{-/-}$, and *Cxcr2*$^{-/-}$ mice treated with acyclovir i.p. daily (n = 10–15/group). Data are presented as mean ± SEM.

(C) Cumulative morbidity is expressed relative to WT mice and presented as mean ± SEM.

(D) Mortality was assessed twice daily in WT, *Ccr2*$^{-/-}$, and *Cxcr2*$^{-/-}$ mice.

(E) Flow cytometry of whole brain was performed at DPI 3 to quantify neutrophil (Ly6G^{hi}/Ly6C^{int}) and inflammatory monocyte (CD11b$^+$/CD45^{hi}) recruitment, expressed as mean ± SEM (n = 6–10 per group).

(F) Plaque assay of whole-brain homogenate at DPI 3, expressed as mean ± SEM (n = 5–11/group).

(G) Confocal microscopy was performed on brain cortex following infection with HSV-1 in CCR2-RFP/CX3CR1-GFP mice on DPI 1 stained *ex vivo* for CD31 and Ly6G to image neutrophil migration, which demonstrated perivascular predominance of Ly6G$^+$ (n = 3, scale bars: 100 and 50 μm).

(H) Mortality and cumulative morbidity after HSV-1 infection was determined with and without neutrophil depletion on DPI −1, 1, and 3. Data are presented as mean ± SEM.

(I) BBB permeability of WT uninfected mice and HSV-infected WT, *Cxcr2*$^{-/-}$, and *Ccr2*$^{-/-}$ mice, shown as mean ± SEM of the brain:serum albumin ratio (n = 3–5/group).

*p < 0.05; **p < 0.01; ***p < 0.001.

The CXCL1-CXCR2 Axis Is Required for Neutrophil Transmigration and Regulates Intra-luminal and Abluminal Migratory Behavior

We assessed the impact of CXCL1/CXCR2 expression on the temporospatial kinetics of neutrophil transendothelial migration and their intra- and extra-vascular migratory behavior. Neutrophils were visualized in *LysM*-GFP mice that either were WT for

Cxcr2 or were *Cxcr2*$^{-/-}$. These mice underwent i.c. HSV-1 or sterile PBS injection, and then cranial window surgery was performed. *LysM*-GFP is expressed by neutrophils and monocytes; therefore, mice were imaged 6–8 h following infection during the early phase of neutrophil migration in response to HSV-1 infection, as identified in the previous flow-cytometry studies. 6–8 h post-infection, mice received Qtracker 605 i.v. to delineate blood
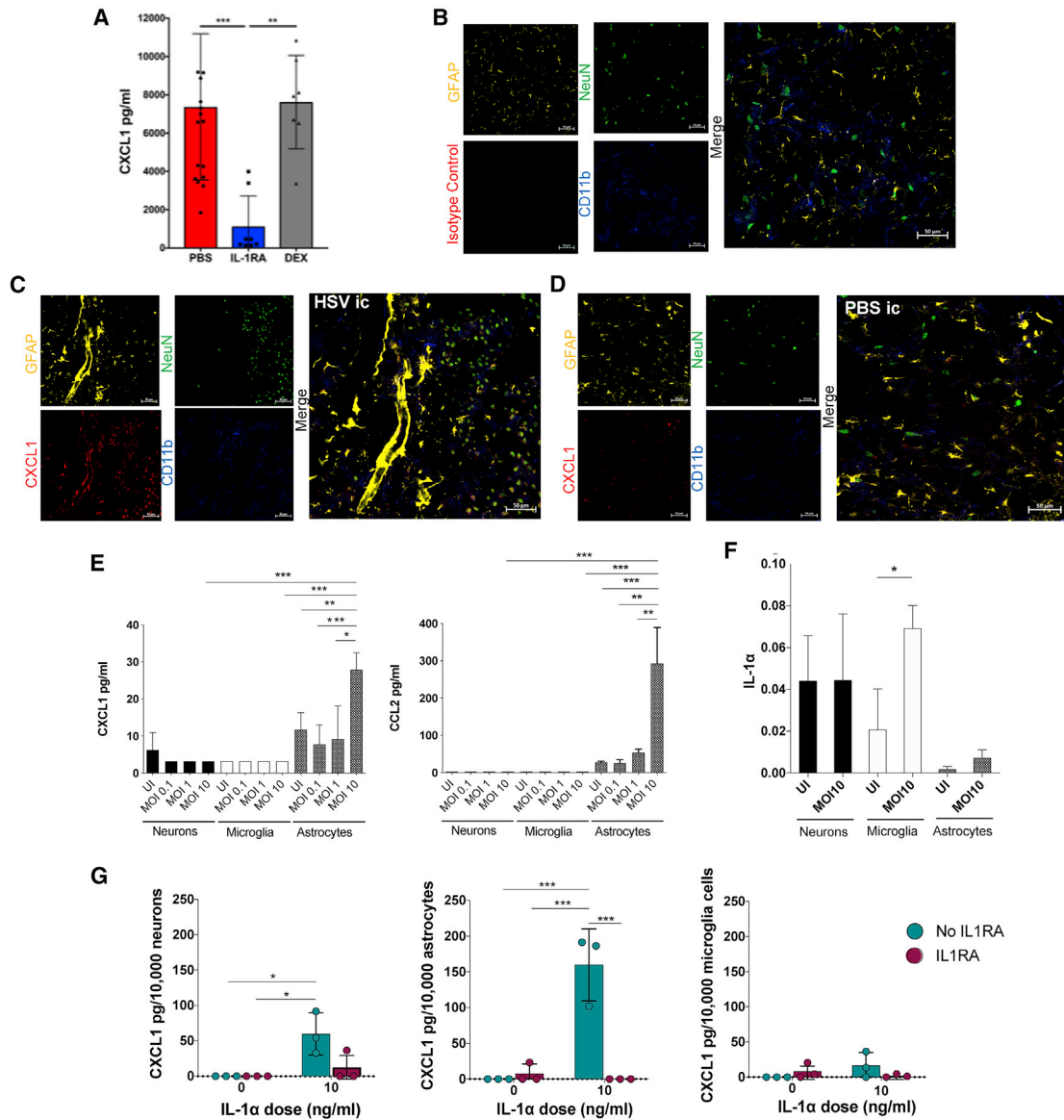
Figure 3. CXCL1 Is Produced by Astrocytes and Neurons

(A) WT mice received IL-1RA or dexamethasone i.p. immediately following HSV-1 i.c. infection, and whole-brain CXCL1 concentration was determined by bead array during DPI 3–5 (n = 7–19/group in duplicate). Data are presented as mean ± SEM.

(B) Confocal microscopy of HSV-1-infected brain sections was performed at DPI 1 following incubation with GFAP, NeuN, CD11b, and isotype control antibodies (scale bar: 50 μm).

(C and D) Confocal microscopy of HSV-1-infected (C) and sham-infected (D) brain sections was performed at DPI 1 following incubation with GFAP, NeuN, CD11b, and CXCL1 antibodies (scale bar: 50 μm).

(E) Primary neurons, microglia, and astrocytes were incubated with HSV-1 for 1 h at a multiplicity of infection (MOI) of 0.1, 1, or 10 or uninfected (UI), and supernatants collected at 24 h were analyzed by Luminex multiplex array. Data are presented as mean ± SD.

(F) Primary neurons, microglia, and astrocytes were incubated with HSV-1 for 1 h at an MOI of 10 or uninfected (UI), RNA was extracted, and IL-1α RNA levels were determined by qRT-PCR and presented as mean ± SD.

(G) Primary neurons, microglia, and astrocytes were stimulated with 10 ng/mL of IL-1α, and CXCL1 production was determined by ELISA. Data are presented as mean ± SD.

*p < 0.05; **p < 0.01; ***p < 0.001.

vessels, and the mice were imaged by intravital microscopy on a custom imaging stage. In sham-PBS-infected *LysM*-GFP mice, *LysM*-GFP+ neutrophils remained predominantly in the intravas-cular space (Figure 4A; Video S1). Following i.c. HSV-1 infection, there was marked transendothelial migration of *LysM*-GFP+ cells through post-capillary venules that was associated both
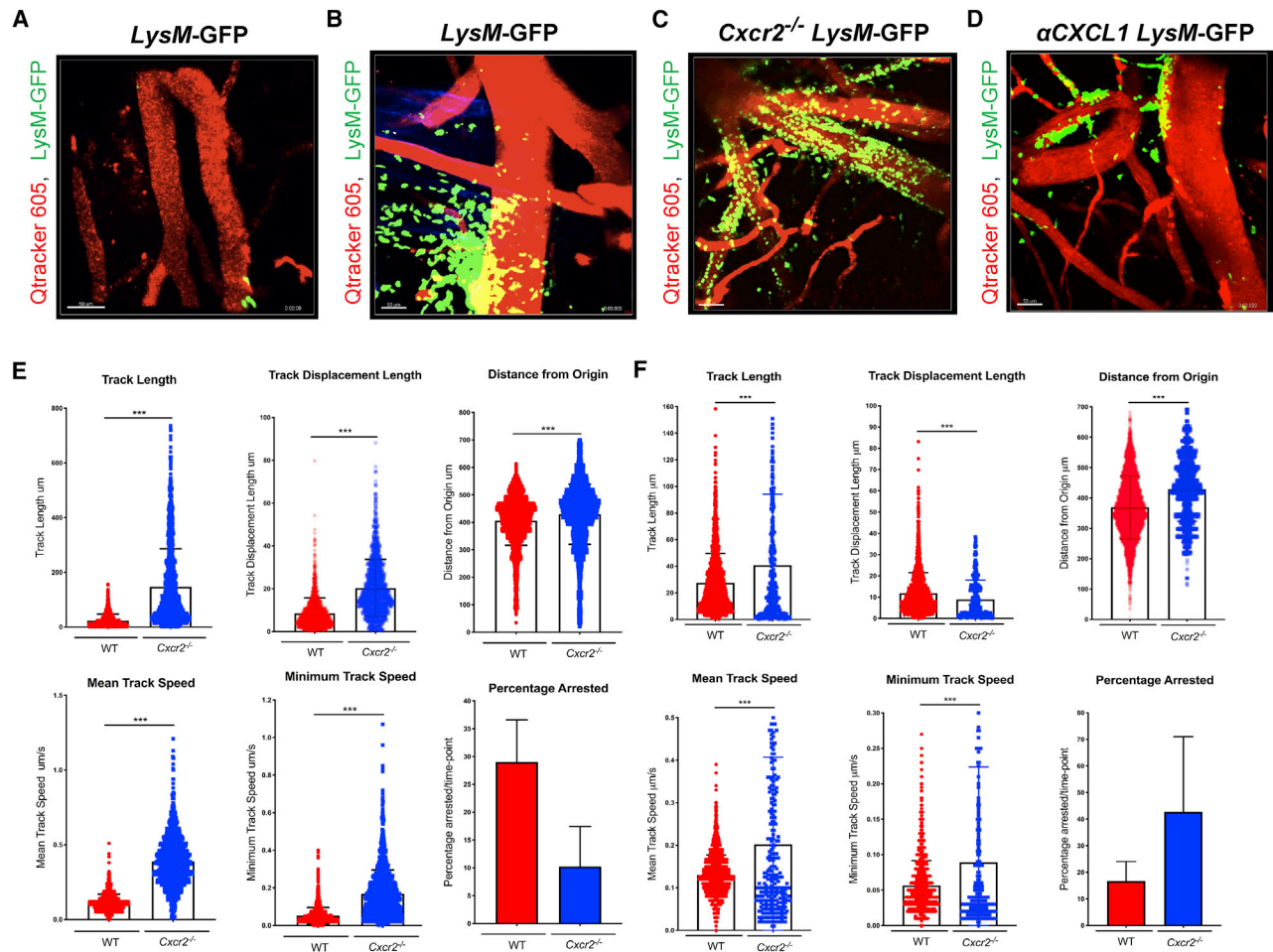
Figure 4. The CXCL1-CXCR2 Axis Is Required for Neutrophil Transmigration and Influences Intra-luminal and Abluminal Migratory Behavior

(A–D) Representative images from supplemental videos. (A) Video S1. *LysM*-GFP mice were imaged using two-photon intravital microscopy immediately following i.v. injection with Qtracker 605, 6–8 h following infection (n = 3/group). Following sterile PBS i.c., minimal intravascular recruitment and extravasation of GFP+ neutrophils were seen. (B) Video S2. *LysM*-GFP mice following i.c. infection with HSV 1 × 10^5 PFU exhibit dramatic extravasation of *LysM*-GFP neutrophils into the brain, with neutrophils displaying swarming and accumulation in the abluminal space. (C) Video S3. *Cxcr2*^−/−^*LysM*-GFP mice infected with HSV show marked recruitment of GFP+ neutrophils to the intravascular space but a striking restriction of extravasation. (D) Video S4. Similarly, in *LysM*-GFP mice that received an αCXCL1 antibody following HSV-1 infection, GFP+ neutrophils are inhibited from significant extravasation.

(E) Baseline Qtracker 605 fluorescence was used to compute the vessel surface and intravascular dynamics determined using Imaris. In the intravascular space, GFP+ neutrophils in *Cxcr2*^−/−^ mice demonstrated significantly longer tracks of greater displacement, with greater mean and minimum speeds and fewer achieving arrest in comparison to WT mice following HSV-1 infection. Data are presented as mean ± SEM.

(F) In the extravascular space, neutrophils in WT mice demonstrated shorter track lengths and decreased distance from their origin, which was associated with slower mean and minimum speeds in comparison to neutrophils in *Cxcr2*^−/−^ mice, reflecting the predilection for most transmigrated neutrophils to be retained in the perivascular abluminal region in WT mice, but not *Cxcr2*^−/−^ mice. Data are presented as mean ± SEM.

*p < 0.05; **p < 0.01; ***p < 0.001.

swarming behavior and a predominant accumulation of GFP+ neutrophils in the perivascular abluminal space (Figure 4B; Video S2). However, this behavior depended on CXCR2 expression. Thus, in *Cxcr2*^−/−^*LysM*-GFP mice infected with HSV-1, GFP+ cells were almost exclusively restricted to the intravascular space, with few achieving transendothelial migration (Figure 4C; Video S3). Similarly, blocking CXCR2-CXCL1 interaction with an αCXCL1 antibody at 2 h after infection reduced neutrophil transendothelial migration (Figure 4D; Video S4). Mice lacking the leukotriene B4 receptor, BLT1, or the complement C5a receptor, C5aR1, which are associated with neutrophil migration and

swarming (Miyabe et al., 2017; Kim et al., 2006; Lämmermann et al., 2013), were studied, but the marked differences in neutrophil transendothelial migration seen in *Cxcr2*^−/−^ mice were not observed in these two mouse strains (data not shown).

To analyze the migratory behavior of *LysM*-GFP+ neutrophils in the intravascular and extravascular spaces, the Qtracker signal was used to compute the vessel surface using Imaris and the spatiotemporal dynamics of GFP+ cells within and outside of the vessel surface were compared, respectively. In the intravascular space, neutrophils in *Cxcr2*^−/−^ mice demonstrated significantly longer tracks of greater displacement, with
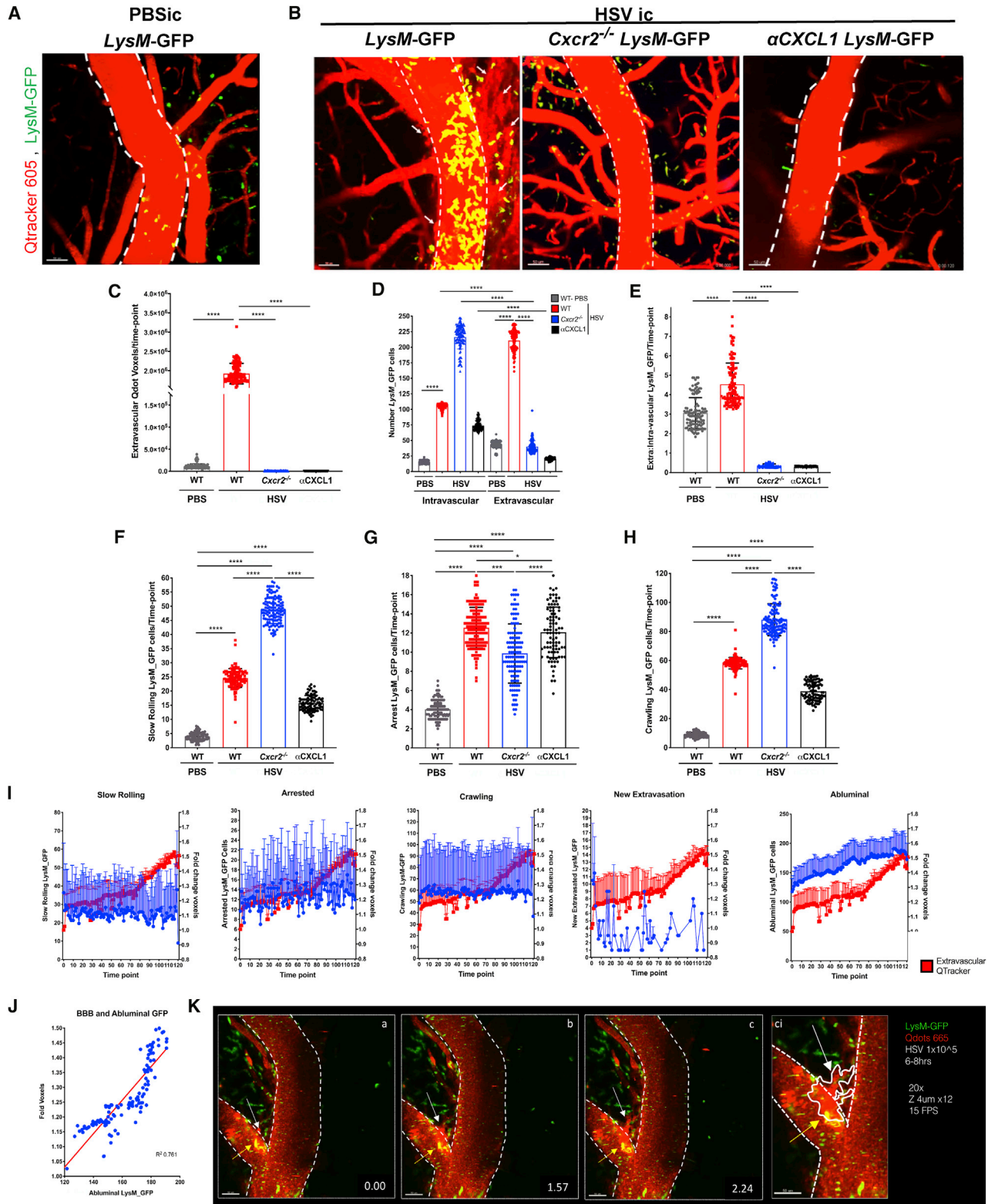
Figure 5. Abrogation of the CXCL1-CXCR2 Axis Reduces BBB Permeability

(A and B) Representative images from supplemental videos (n = 3/group). (A) Video S5. 6–8 h following sterile PBS i.c. injection into *LysM*-GFP mice. (B) Videos S6, S7, and S8. Following HSV-1 i.c. infection into *LysM*-GFP mice, extensive leakage of Qtracker 605 can be seen, reflecting BBB permeability (Video S6),

(legend continued on next page)

greater mean and minimum speeds and fewer achieving arrest in comparison to WT mice following i.c. HSV-1 infection (Figure 4E). In the extravascular space, transmigrated neutrophils in WT mice demonstrated reduced distance from their origin, which was associated with slower mean and minimum speeds in comparison to neutrophils in Cxcr2$^{-/-}$ mice (Figure 4F). This reflected the predilection for most transmigrated neutrophils to be retained in the perivascular abluminal region in WT mice, but not Cxcr2$^{-/-}$ mice, during early disease.

Abrogation of the CXCL1-CXCR2 Axis Reduces BBB Permeability

To assess the impact of this altered migratory behavior on BBB permeability, the volume of extravascular Qtracker 605 leakage was visualized. To determine the vessel surface, the baseline Qtracker 605 signal was computed to create a surface using Imaris. In sham-infected WT mice, minimal Qtracker leakage was seen (Figure 5A; Video S5). However, following i.c. HSV-1 infection, marked Qtracker leakage was seen, indicating an increase in BBB permeability (Figure 5B; Video S6). Interestingly, in Cxcr2$^{-/-}$ mice and WT mice treated i.v. with αCXCL1, HSV-1 infection was not associated with Qtracker leakage (Figure 5B; Videos S7 and S8). For quantitative analysis, again the baseline Qtracker signal was used to establish the vessel surface, and the volume of Qtracker outside of the computed vessel surface was measured in voxels to quantify BBB permeability. The extravasated Qdot voxels were quantified for sham-infected WT, HSV-infected WT, and HSV-infected Cxcr2$^{-/-}$ mice and for HSV-infected WT mice treated with αCXCL1 antibody (Figure 5C). We observed that as previously shown (Figures 1C–1E and 2I), HSV-1 infection led to increased BBB permeability; however, the integrity of the BBB was not compromised during infection of Cxcr2$^{-/-}$ mice or in WT mice treated with αCXCL1 antibody.

To determine the impact of CXCR2 and CXCL1 on neutrophil extravasation, the number of LysM-GFP+ cells was determined within and outside of the computed vessel surface at each time point using Imaris. Following i.c. HSV-1 infection, there was both an increase in intravascular GFP+ neutrophil recruitment and a marked increase in extravascular GFP+ cell accumulation in WT mice (Figure 5D). However, in Cxcr2$^{-/-}$LysM-GFP mice, the converse was seen, with a dramatic reduction in extravascular GFP+ neutrophils and a relative increase in GFP+ cells restricted to the intravascular space. Similarly, fewer extrava-

sated GFP+ cells were identified in WT mice treated with αCXCL1 relative to the intravascular cells. To more accurately quantitate the relative extravasation between the groups, the intravascular-to-extravascular LysM-GFP ratio was calculated. These analyses showed a significant reduction in the proportion of extravasated LysM-GFP+ neutrophils in both Cxcr2$^{-/-}$ mice and αCXCL1 antibody-treated WT mice (Figure 5E).

To interrogate the specific phases of migration that best correlated with BBB breakdown, the number of LysM-GFP+ neutrophils that exhibited slow rolling, arrest, and crawling at each time point was determined (Phillipson et al., 2009). In comparison to sham infection with sterile PBS, HSV-1 infection was associated with an increase in the number of neutrophils at each stage of migration (Figures 5F–5H). However, in Cxcr2$^{-/-}$ mice, there was a reduction in the number that achieved arrest and a corresponding increase in the number of slow rolling GFP+ neutrophils. In addition, there was an increased number of GFP+ neutrophils crawling within the blood vessel lumen at each time point in Cxcr2$^{-/-}$ mice, reflecting impaired transendothelial migration (Figure 5H). The i.v. injection of αCXCL1, 2 h following infection, in WT mice did not significantly change the number of slow rolling cells (Figure 5F) and was associated with a more modest reduction in the number of GFP+ neutrophils that arrested than was observed in Cxcr2$^{-/-}$ mice (Figure 5G). Altogether, these data suggest that neutrophil CXCR2 expression is required for both arrest and transendothelial migration and that reduced numbers of neutrophils seen achieving arrest results in correspondingly greater numbers observed slow rolling. In addition, of the limited number of neutrophils that arrest, a greater number are seen crawling because of impaired transendothelial migration. Finally, treatment with an αCXCL1 antibody also partially reduced neutrophil arrest, although not to the same extent as Cxcr2 deficiency, whereas the αCXCL1 antibody was as effective at inhibiting neutrophil transendothelial migration as Cxcr2 deficiency. These data suggest that although CXCL1 has a non-redundant function in arrest in this model, other CXCR2 ligands likely contribute to arrest. Nevertheless, CXCL1 is the main CXCR2 ligand required for neutrophil transendothelial migration.

Progressive Qtracker leakage over time was analyzed in LysM-GFP mice in comparison to neutrophil slow rolling, arrest, crawling, new extravasation, and total abluminal cell count over time. Of these parameters, only the total number of abluminal

whereas in Cxcr2$^{-/-}$LysM-GFP mice, HSV-1 infection does not induce Qtracker 605 leakage (Video S7). Similarly, administration of i.v. αCXCL1 into LysM-GFP mice 2 h following infection abrogates Qtracker 605 leakage (Video S8).

(C) Volume of Qtracker leakage outside of the vessel surface was determined at each time point, confirming significant amelioration of BBB permeability in Cxcr2$^{-/-}$LysM-GFP mice and in LysM-GFP mice following i.v. αCXCL1. Data shown are representative of 3 independent experiments.

(D) Total number of LysM-GFP+ neutrophils in the intravascular and extravascular spaces was determined by calculating those within and outside of the computed vessel surface, respectively.

(E) These data are expressed as the intravascular:extravascular ratio, demonstrating marked reduction in extravasation of GFP+ neutrophils in Cxcr2$^{-/-}$LysM-GFP mice and in LysM-GFP mice following i.v. αCXCL1.

(F–H) Number of intravascular GFP+ cells that were (F) slow rolling, (G) arrested, or (H) crawling at each time point was computed by Imaris, showing a reduction in GFP+ cell arrest in Cxcr2$^{-/-}$LysM-GFP mice and to a lesser extent in LysM-GFP mice following i.v. αCXCL1 and a relative increase in the number of cells slow rolling and crawling in Cxcr2$^{-/-}$ mice.

(I and J) Slow rolling, arrest, crawling, new extravasation, and abluminal numbers of GFP+ cells (blue) in LysM-GFP mice were expressed relative to Qtracker 605 leakage (red) over time, demonstrating that only the number of abluminal GFP+ cells correlated with BBB permeability.

(K) Film strip image from Video S9, demonstrating perivascular crawling of an extravasated LysM-GFP+ neutrophil (yellow arrow) and subsequent Qtracker 605 leakage (white arrow).

All data in this figure are presented as mean ± SEM. *p < 0.05; **p < 0.01; ***p < 0.001; ****p < 0.0001.

LysM-GFP+ cells increased correspondingly with BBB permeability over time (Figure 5I), and this directly correlated with Qtracker leakage at any time point (Figure 5J). This suggested that neutrophil transmigration was temporally and spatially associated with BBB permeability. The latter process was visualized in a representative movie of three experiments during which an extravasated neutrophil was monitored and demonstrated abluminal crawling before Qtracker leakage, suggesting that the presence of transmigrated neutrophils in the perivascular space can directly increase BBB permeability (Figure 5K; Video S9).

DISCUSSION

Our work demonstrates that following i.c. infection with HSV-1, the virus localized to the hippocampus and was accompanied by a cascade of chemokines, particularly CXCL1 and CCL2, that drove the migration of neutrophils and inflammatory monocytes into the brain, respectively. Remarkably, the migration of these innate immune cells continued despite the enhanced clearance of virus with acyclovir. We have found that abrogation of CCL2-CCR2 signaling was associated with diminished monocyte recruitment, increased viral load, and increased morbidity. Conversely, abrogation of CXCL1-CXCR2 signaling was associated with diminished neutrophil migration into the brain, decreased BBB permeability, and reduced morbidity but did not significantly alter viral load. Using intravital microscopy, we demonstrated that HSV-1 infection led to transmigration of neutrophils and perivascular swarming, which depended on CXCL1-CXCR2 signaling. CXCL1 was produced by perivascular astrocytes in response to HSV-1 and by both astrocytes and neurons in response to microglia-derived IL-1α. Abrogation of this chemokine pathway attenuated neutrophil arrest, transmigration, and the breakdown of the BBB. Specifically, CXCL1 exerted a modest effect on neutrophil arrest but was critical for the transendothelial migration and abluminal accumulation of neutrophils, which correlated with increased BBB permeability. Altogether, these results argue that despite acyclovir treatment, the recruitment of CCR2^{+} inflammatory monocytes is critical for the control of HSV-1, whereas CXCR2^{+} neutrophil transmigration is not required for the control of viral replication and contributes to the immunopathogenesis of the condition.

A previous study used corneal scarification to inoculate HSV-1 and observed that the administration of acyclovir from 24 h following detection of virus in the central nervous system (CNS) did not reduce either mortality or CD45^{hi} inflammatory infiltrate (Lundberg et al., 2008). During localized corneal infection with HSV-1, neutrophil migration and keratitis were reduced following administration of anti-CXCL1 monoclonal antibody and in *Cxcr2*^{−/−} mice (West et al., 2014); however, the role of CXCL1-CXCR2 in the CNS response to HSV-1 infection has been unclear. CXCL1 expression in the CNS has also been seen in response to i.p. lipopolysaccharide injection in mice and to pneumococcal CNS infection in Wistar rats, which was associated with breakdown of the BBB (McKimmie and Graham, 2010; Barichello et al., 2012; Roy et al., 2012). However, chemokine expression by specific neuroglial cells, particularly in response to viral infection, has been less frequently studied. Dengue virus i.c. infection has been demonstrated to induce

the expression of multiple chemokines and leukocyte adhesion to endothelium, although the critical receptor-ligand interactions driving leukocyte transendothelial migration and increased BBB permeability were not elucidated (Amaral et al., 2011).

We also observed that following infection with HSV-1, CXCL1 expression by neurons and astrocytes, as opposed to microglia, increased as observed by the co-localization of CXCL1 with GFAP[+] perivascular astrocytes and NeuN[+]-expressing neurons *in vivo*. CXCL1 has not previously been shown to co-localize with astrocytes following HSV-1 infection, although this has been reported in response to mouse hepatitis virus infection and NMDA stimulation of corticostriatal slice cultures (Hosking et al., 2009; Katayama et al., 2009; Mancini and Vidal, 2018). Nevertheless, microglia are important resident CNS immune cells and produce a robust inflammatory cytokine response to HSV-1 *in vitro* (Marques et al., 2006). CXCL1 expression has also been reported to be expressed by activated microglia, pericytes, and endothelial cells in response to non-HSV-1 stimuli (Marques et al., 2006; Semple et al., 2010; Kim and Luster, 2015). However, astrocytes ensheath most cerebral blood vessels, together with pericytes, forming a critical component of the BBB and are capable of inflammatory cytokine production (Liddelow et al., 2017). It has been postulated that transmigrated leukocytes migrate in response to local chemokine gradients, and here we have shown that the principle chemokine produced in response to HSV-1 infection also co-localizes with astrocytes lining the perivascular space in which transmigrated neutrophils accumulate (Weninger et al., 2014).

Interestingly, we found that stimulation of neurons and astrocytes with IL-1α increased the expression of CXCL1 and that the administration of IL-1RA resulted in a marked decrease in CXCL1 production, suggesting that neuronal and astrocytic CXCL1 expression is IL-1 dependent. IL-1 can be produced by microglia following recognition of HSV-1 pathogen-associated molecular patterns by TLR2 and TLR9 (Wuest and Carr, 2008; Piret and Boivin, 2015; Marques et al., 2004), and we confirmed that HSV-1 infection increases IL-1α production by microglia. It has been demonstrated that *in vitro* stimulation of purified astrocytes produce a range of inflammatory mediators in response to a microglia-derived cytokine cocktail containing IL-1 (Liddelow et al., 2017). In addition, the production of TLR2-driven inflammatory mediators in purified astrocyte cultures depends on the paracrine expression of IL-1β by microglia in experimental spinal cord injury (Rubio and Sanz-Rodriguez, 2007; Pineau et al., 2010; Facci et al., 2014). In addition, the administration of IL-1 in a murine stroke model is associated with upregulation of several mediators, including CXCL1, increased neutrophil recruitment, and a greater volume of ischemic injury; consequently, IL-1RA has been explored in clinical trials of stroke. However, initial evidence of efficacy in murine models of stroke-induced inflammation have not been borne out in clinical trials, partly because of the short-term and paracrine actions of IL-1 (McColl et al., 2007; Smith et al., 2018). Nevertheless, the therapeutic potential of IL-1 antagonism may be limited by the importance of IL-1 and tumor necrosis factor alpha (TNF-α) expression in mitigating viral replication (Sergerie et al., 2007). Moreover, although delayed post-infection corticosteroid therapy has been associated with reduced cerebral edema in

experimental HSV-1 encephalitis, we found sustained production of CXCL1 when dexamethasone was given acutely during HSV-1 infection, suggesting that more targeted therapies are required (Meyding-Lamadé et al., 2003).

We found that CXCR2 was critical for neutrophil arrest and transendothelial migration and that $Cxcr2^{-/-}$ mice demonstrated reduced BBB permeability during HSV-1 infection. However, although CXCL1 exerted a moderate effect on neutrophil arrest, it was crucial for transendothelial migration, which was associated with breakdown of the BBB. Our results further suggest that injury to the BBB can occur in association with the presence of abluminal neutrophil retention. There is growing interest in the potential of this perivenular space between the astrocyte endfeet of the glia limitans and the abluminal surface of the vascular endothelium as an immunological niche (Coles et al., 2017). Here we demonstrate that extravasated neutrophils accumulate in this space and, in doing so, they may be contributing to secondary BBB breakdown, which was abrogated in $Cxcr2^{-/-}$ mice or following αCXCL1 (Coles et al., 2017). It has been shown that CXCR2 is critical for transendothelial migration and survival of neutrophils in models of immune complex-induced arthritis and TNF-induced cremaster inflammation (Miyabe et al., 2017, 2019; Girbl et al., 2018). Our data suggest that the relative contribution of CXCR2 ligands may be context dependent, because in the cremaster model, CXCL1 is required for neutrophil arrest and CXCL2 is required for transendothelial migration (Girbl et al., 2018). However, the discrepancy in the relative importance of CXCL1 on neutrophil transendothelial migration may reflect the predominant expression of CXCL1 by endothelial cells during TNF stimulation of cremaster muscle, as opposed to the predominant extra-luminal expression of CXCL1 by astrocytes and neurons that, along with endothelial tight junctions in the CNS, may produce a spatially distinct CXCL1 chemokine gradient (Kim and Luster, 2015; Filippi, 2019). We speculate that CXCL1 could still contribute to neutrophil arrest from this compartment following transport into the blood vessel lumen by the atypical chemokine receptor ACKR1, as has been demonstrated in a model of inflammatory arthritis (Miyabe et al., 2019).

Following non-lethal LCMV infection in mice, it was elegantly demonstrated that neutrophils and monocytes transmigrate toward infected perivascular fibroblasts and that this is associated with BBB leakage (Kim et al., 2009). Here we identify that the pivotal chemokine in this process during HSV-1 infection is CXCL1 and that it is not arrest but both transendothelial migration and perivascular abluminal accumulation of neutrophils that are spatially and temporally associated with injury to the BBB. The exact mechanisms by which abluminal neutrophils contribute to breakdown of the BBB requires study. However, transendothelial migration of neutrophils has been associated with neurotoxicity, release of proteases, loss of tight junction proteins, and production of neutrophil extracellular traps (Bolton et al., 1998; Allen et al., 2012; Finsterbusch et al., 2014; Weninger et al., 2014; de Buhr et al., 2017). In addition, *in vivo* models of ischemia/reperfusion injury have identified that post-migration neutrophil elastase production plays a vital role in remodeling of the venular basement membrane (Voisin et al., 2019). In addition, transmigrated neutrophils demonstrate upregulated expression of CXCL2 and CCL2, suggesting that the abluminal

presence of perivascular neutrophils may perpetuate additional neutrophil and monocyte transendothelial migration, with the possibility of vicious neutrophil-monocyte crosstalk that leads to increased neuronal and BBB damage (Chou et al., 2010; Li et al., 2016; Soehnlein et al., 2017; Weninger et al., 2014). It seems likely that the relative contribution of CXCR2 signaling to neuropathology and mortality depends on the primary population of infected cells and the chronology of infection. For example, in West Nile virus encephalitis, CXCR2+ neutrophils serve as a reservoir for early viral dissemination into the CNS but are later required for effective viral clearance (Bai et al., 2010; Wang et al., 2012), whereas HSV-1, along with many other viruses causing encephalitis, does not require neutrophils for migration into the CNS and instead establishes CNS infection following neuronal transportation (Smith et al., 2001). Neutrophil swarming behavior has been reported in several organs, including lymph nodes, lung, and skin, in response to bacterial or parasite infection. Here we identified perivascular neutrophil swarming in response to viral infection in the brain in regions of increased BBB permeability, potentially reflecting remodeling of the extravascular matrix (Kienle and Lämmermann, 2016). Nevertheless, the impact of neutrophil migration appears to be context dependent, because an inducible astrocyte-specific CXCL1 transgenic model resulted in increased neutrophil migration, which was associated with demyelination, but not a breakdown of the BBB (Marro et al., 2016; Grist et al., 2018). In contrast, in a transgenic model of oligodendrocyte-specific CXCL1 constitutive expression, neutrophil infiltration into the brain was associated with disruption of the BBB and increased mortality without dysmyelination (Tani et al., 1996).

Neutrophil depletion before i.c. infection with the neurotropic JHM strain of mouse hepatitis virus has been associated with reduced BBB permeability in a mouse model, although receptor/ligand interactions and migratory dynamics were not established (Zhou et al., 2003). Similarly, depletion of neutrophils in a model of experimental autoimmune myelitis has been associated with reduced spinal cord BBB compromise, and $IL-1r1^{-/-}$ mice exhibited reduced neutrophil arrest (Carlson et al., 2008; Aubé et al., 2014). Here we identify that CXCL1 is the major CXCR2 ligand upregulated in the brain during HSV-1 encephalitis, can be inhibited by IL-1RA, and is critical for the neutrophil transendothelial migration and abluminal accumulation, which correlates with BBB permeability. αCXCL1 antibody treatment only exhibited a partial effect on neutrophil arrest relative to CXCR2 deficiency, which may reflect a role for additional CXCR2 ligands in arrest, such as CXCL2, or may reflect a difference in efficacy between genetic deficiency and antibody-mediated inhibition.

Overall, our work demonstrates that during HSV-1 encephalitis, despite viral clearance with acyclovir, IL-1-dependent CXCL1 production from perivascular astrocytes and neurons plays a pivotal role in the CXCR2-dependent transendothelial migration of neutrophils into the brain and their accumulation in the abluminal space. These recruited neutrophils are likely key drivers of increased BBB permeability, which is associated with increased morbidity and mortality. Thus, blockade of the CXCL1-CXCR2 chemokine axis could be a therapeutic approach to attenuate CNS injury in HSV-1 encephalitis by inhibiting neutrophil recruitment into the brain.

STAR★METHODS

Detailed methods are provided in the online version of this paper and include the following:

- KEY RESOURCES TABLE
- RESOURCE AVAILABILITY
  - Lead contact
  - Materials availability
  - Data and code availability
- EXPERIMENTAL MODEL AND SUBJECT DETAILS
  - HSV strains
  - Mice and infection model
  - Primary cell cultures
  - Cell lines
- METHOD DETAILS
  - Neurological Disease Severity score and Evans Blue assessment of BBB permeability
  - Flow cytometry
  - Luminex bead-based multiplex assay
  - Plaque assay
  - Confocal microscopy
  - Wide-field microscopy
  - *In vitro* infection of primary cells
  - Cranial window surgery and multi-photon intravital microscopy
  - Reverse Transcription Quantitative PCR (RT-qPCR)
  - Mouse Primers
  - Neutrophil depletion
- QUANTIFICATION AND STATISTICAL ANALYSES

AUTHOR CONTRIBUTIONS

B.D.M. and A.D.L. designed the research, and B.D.M. and L.B.-M. conducted the experiments. B.D.M. and L.B.-M. conducted data analysis, and B.D.M., A.D.L., and E.A.K.-J. wrote the paper, with significant critical input from L.B.-M., E.S., J.L., Y.M., and T.S.

REFERENCES

Allen, C., Thornton, P., Denes, A., McColl, B.W., Pierozynski, A., Monestier, M., Pinteaux, E., Rothwell, N.J., and Allan, S.M. (2012). Neutrophil cerebrovascular transmigration triggers rapid neurotoxicity through release of proteases associated with decondensed DNA. J. Immunol. *189*, 381–392.

Amaral, D.C., Rachid, M.A., Vilela, M.C., Campos, R.D., Ferreira, G.P., Rodrigues, D.H., Lacerda-Queiroz, N., Miranda, A.S., Costa, V.V., Campos, M.A., et al. (2011). Intracerebral infection with dengue-3 virus induces meningoencephalitis and behavioral changes that precede lethality in mice. J. Neuroinflammation *8*, 23.

Aubé, B., Lévesque, S.A., Paré, A., Chamma, É., Kébir, H., Gorina, R., Lécuyer, M.A., Alvarez, J.I., De Koninck, Y., Engelhardt, B., et al. (2014). Neutrophils mediate blood-spinal cord barrier disruption in demyelinating neuroinflammatory diseases. J. Immunol. *193*, 2438–2454.

Bai, F., Kong, K.F., Dai, J., Qian, F., Zhang, L., Brown, C.R., Fikrig, E., and Montgomery, R.R. (2010). A paradoxical role for neutrophils in the pathogenesis of West Nile virus. J. Infect. Dis. *202*, 1804–1812.

Barichello, T., Generoso, J.S., Silvestre, C., Costa, C.S., Carradore, M.M., Cipriano, A.L., Michelon, C.M., Petronilho, F., Dal-Pizzol, F., Vilela, M.C., and Teixeira, A.L. (2012). Circulating concentrations, cerebral output of the CINC-1 and blood–brain barrier disruption in Wistar rats after pneumococcal meningitis induction. Eur. J. Clin. Microbiol. Infect. Dis. *31*, 2005–2009.

Barnett, E.M., Jacobsen, G., Evans, G., Cassell, M., and Perlman, S. (1994). Herpes simplex encephalitis in the temporal cortex and limbic system after trigeminal nerve inoculation. J. Infect. Dis. *169*, 782–786.

Bennett, J., Basivireddy, J., Kollar, A., Biron, K.E., Reickmann, P., Jefferies, W.A., and McQuaid, S. (2010). Blood-brain barrier disruption and enhanced vascular permeability in the multiple sclerosis model EAE. J. Neuroimmunol. *229*, 180–191.

Boivin, N., Menasria, R., Gosselin, D., Rivest, S., and Boivin, G. (2012). Impact of deficiency in CCR2 and CX3CR1 receptors on monocytes trafficking in herpes simplex virus encephalitis. J. Gen. Virol. *93*, 1294–1304.

Bolton, S.J., Anthony, D.C., and Perry, V.H. (1998). Loss of the tight junction proteins occludin and zonula occludens-1 from cerebral vascular endothelium during neutrophil-induced blood-brain barrier breakdown *in vivo*. Neuroscience *86*, 1245–1257.

Brockman, M.A., and Knipe, D.M. (2002). Herpes simplex virus vectors elicit durable immune responses in the presence of preexisting host immunity. J. Virol. *76*, 3678–3687.

Cacalano, G., Lee, J., Kikly, K., Ryan, A.M., Pitts-Meek, S., Hultgren, B., Wood, W.I., and Moore, M.W. (1994). Neutrophil and B cell expansion in mice that lack the murine IL-8 receptor homolog. Science *265*, 682–684.

Carlson, T., Kroenke, M., Rao, P., Lane, T.E., and Segal, B. (2008). The Th17-ELR+ CXC chemokine pathway is essential for the development of central nervous system autoimmune disease. J. Exp. Med. *205*, 811–823.

Chou, R.C., Kim, N.D., Sadik, C.D., Seung, E., Lan, Y., Byrne, M.H., Haribabu, B., Iwakura, Y., and Luster, A.D. (2010). Lipid-cytokine-chemokine cascade drives neutrophil recruitment in a murine model of inflammatory arthritis. Immunity *33*, 266–278.

Coles, J.A., Myburgh, E., Brewer, J.M., and McMenamin, P.G. (2017). Where are we? The anatomy of the murine cortical meninges revisited for intravital imaging, immunology, and clearance of waste from the brain. Prog. Neurobiol. *156*, 107–148.

Colgrove, R.C., Liu, X., Griffiths, A., Raja, P., Deluca, N.A., Newman, R.M., Coen, D.M., and Knipe, D.M. (2016). History and genomic sequence analysis of the herpes simplex virus 1 KOS and KOS1.1 sub-strains. Virology 487, 215–221.

Conrady, C.D., Zheng, M., Mandal, N.A., van Rooijen, N., and Carr, D.J. (2013). IFN-α-driven CCL2 production recruits inflammatory monocytes to infection site in mice. Mucosal Immunol. 6, 45–55.

de Buhr, N., Reuner, F., Neumann, A., Stump-Guthier, C., Tenenbaum, T., Schroten, H., Ishikawa, H., Müller, K., Beineke, A., Hennig-Pauka, I., et al. (2017). Neutrophil extracellular trap formation in the Streptococcus suis-infected cerebrospinal fluid compartment. Cell. Microbiol. 19, 1–16.

Desai, P., DeLuca, N.A., and Person, S. (1998). Herpes simplex virus type 1 VP26 is not essential for replication in cell culture but influences production of infectious virus in the nervous system of infected mice. Virology 247, 115–124.

Facci, L., Barbierato, M., Marinelli, C., Argentini, C., Skaper, S.D., and Giusti, P. (2014). Toll-like receptors 2, -3 and -4 prime microglia but not astrocytes across central nervous system regions for ATP-dependent interleukin-1β release. Sci. Rep. 4, 6824.

Faust, N., Varas, F., Kelly, L.M., Heck, S., and Graf, T. (2000). Insertion of enhanced green fluorescent protein into the lysozyme gene creates mice with green fluorescent granulocytes and macrophages. Blood 96, 719–726.

Filippi, M.D. (2019). Neutrophil transendothelial migration: updates and new perspectives. Blood 133, 2149–2158.

Finsterbusch, M., Voisin, M.B., Beyrau, M., Williams, T.J., and Nourshargh, S. (2014). Neutrophils recruited by chemoattractants in vivo induce microvascular plasma protein leakage through secretion of TNF. J. Exp. Med. 211, 1307–1314.

Girbl, T., Lenn, T., Perez, L., Rolas, L., Barkaway, A., Thiriot, A., Del Fresno, C., Lynam, E., Hub, E., Thelen, M., et al. (2018). Distinct Compartmentalization of the Chemokines CXCL1 and CXCL2 and the Atypical Receptor ACKR1 Determine Discrete Stages of Neutrophil Diapedesis. Immunity 49, 1062–1076.e6.

Grist, J.J., Marro, B., and Lane, T.E. (2018). Neutrophils and viral-induced neurologic disease. Clin. Immunol. 189, 52–56.

Grygorczuk, S., Świerzbińska, R., Kondrusik, M., Dunaj, J., Czupryna, P., Moniuszko, A., Siemieniako, A., and Pancewicz, S. (2018). The intrathecal expression and pathogenetic role of Th17 cytokines and CXCR2-binding chemokines in tick-borne encephalitis. J. Neuroinflammation 15, 115.

Hosking, M.P., Liu, L., Ransohoff, R.M., and Lane, T.E. (2009). A protective role for ELR+ chemokines during acute viral encephalomyelitis. PLoS Pathog. 5, e1000648.

Howe, C.L., Lafrance-Corey, R.G., Sundsbak, R.S., and Lafrance, S.J. (2012). Inflammatory monocytes damage the hippocampus during acute picornavirus infection of the brain. J. Neuroinflammation 9, 50.

Katayama, T., Tanaka, H., Yoshida, T., Uehara, T., and Minami, M. (2009). Neuronal injury induces cytokine-induced neutrophil chemoattractant-1 (CINC-1) production in astrocytes. J. Pharmacol. Sci. 109, 88–93.

Kienle, K., and Lämmermann, T. (2016). Neutrophil swarming: an essential process of the neutrophil tissue response. Immunol. Rev. 273, 76–93.

Kim, N.D., and Luster, A.D. (2015). The role of tissue resident cells in neutrophil recruitment. Trends Immunol. 36, 547–555.

Kim, N.D., Chou, R.C., Seung, E., Tager, A.M., and Luster, A.D. (2006). A unique requirement for the leukotriene B4 receptor BLT1 for neutrophil recruitment in inflammatory arthritis. J. Exp. Med. 203, 829–835.

Kim, J.V., Kang, S.S., Dustin, M.L., and McGavern, D.B. (2009). Myelomonocytic cell recruitment causes fatal CNS vascular injury during acute viral meningitis. Nature 457, 191–195.

Klein, R.S., and Hunter, C.A. (2017). Protective and pathological immunity during Central Nervous System Infections. Immunity 46, 891–909.

Kurt-Jones, E.A., Chan, M., Zhou, S., Wang, J., Reed, G., Bronson, R., Arnold, M.M., Knipe, D.M., and Finberg, R.W. (2004). Herpes simplex virus 1 interaction with Toll-like receptor 2 contributes to lethal encephalitis. Proc. Natl. Acad. Sci. USA 101, 1315–1320.

Lämmermann, T., Afonso, P.V., Angermann, B.R., Wang, J.M., Kastenmüller, W., Parent, C.A., and Germain, R.N. (2013). Neutrophil swarms require LTB4 and integrins at sites of cell death in vivo. Nature 498, 371–375.

Li, J.L., Lim, C.H., Tay, F.W., Goh, C.C., Devi, S., Malleret, B., Lee, B., Bakocevic, N., Chong, S.Z., Evrard, M., et al. (2016). Neutrophils Self-Regulate Immune Complex-Mediated Cutaneous Inflammation through CXCL2. J. Invest. Dermatol. 136, 416–424.

Liddelow, S.A., Guttenplan, K.A., Clarke, L.E., Bennett, F.C., Bohlen, C.J., Schirmer, L., Bennett, M.L., Münch, A.E., Chung, W.S., Peterson, T.C., et al. (2017). Neurotoxic reactive astrocytes are induced by activated microglia. Nature 541, 481–487.

Lundberg, P., Ramakrishna, C., Brown, J., Tyszka, J.M., Hamamura, M., Hinton, D.R., Kovats, S., Nalcioglu, O., Weinberg, K., Openshaw, H., and Cantin, E.M. (2008). The immune response to herpes simplex virus type 1 infection in susceptible mice is a major cause of central nervous system pathology resulting in fatal encephalitis. J. Virol. 82, 7078–7088.

Mancini, M., and Vidal, S.M. (2018). Insights into the pathogenesis of herpes simplex encephalitis from mouse models. Mamm. Genome 29, 425–445.

Marques, C.P., Hu, S., Sheng, W., Cheeran, M.C., Cox, D., and Lokensgard, J.R. (2004). Interleukin-10 attenuates production of HSV-induced inflammatory mediators by human microglia. Glia 47, 358–366.

Marques, C.P., Hu, S., Sheng, W., and Lokensgard, J.R. (2006). Microglial cells initiate vigorous yet non-protective immune responses during HSV-1 brain infection. Virus Res. 121, 1–10.

Marro, B.S., Grist, J.J., and Lane, T.E. (2016). Inducible expression of CXCL1 within the central nervous system amplifies viral-induced demyelination. J. Immunol. 196, 1855–1864.

Masanti, I., and Weller, R.O. (2004). Inflammatory Diseases of the CNS I: Encephalitis. Adv. Clin. Neurosci. Rehabil. 4, 23–26.

McColl, B.W., Rothwell, N.J., and Allan, S.M. (2007). Systemic inflammatory stimulus potentiates the acute phase and CXC chemokine responses to experimental stroke and exacerbates brain damage via interleukin-1- and neutrophil-dependent mechanisms. J. Neurosci. 27, 4403–4412.

McKimmie, C.S., and Graham, G.J. (2010). Astrocytes modulate the chemokine network in a pathogen-specific manner. Biochem. Biophys. Res. Commun. 394, 1006–1011.

Menasria, R., Canivet, C., Piret, J., Gosselin, J., and Boivin, G. (2016). Both Cerebral and Hematopoietic Deficiencies in CCR2 Result in Uncontrolled Herpes Simplex Virus Infection of the Central Nervous System in Mice. PLoS ONE 11, e0168034.

Meyding-Lamadé, U.K., Oberlinner, C., Rau, P.R., Seyfer, S., Heiland, S., Sellner, J., Wildemann, B.T., and Lamadé, W.R. (2003). Experimental herpes simplex virus encephalitis: a combination therapy of acyclovir and glucocorticoids reduces long-term magnetic resonance imaging abnormalities. J. Neurovirol. 9, 118–125.

Michael, B.D., Griffiths, M.J., Granerod, J., Brown, D., Davies, N.W.S., Borrow, R., and Solomon, T. (2016a). Characteristic Cytokine and Chemokine Profiles in Encephalitis of Infectious, Immune-Mediated, and Unknown Aetiology. PLoS ONE 11, e0146288.

Michael, B.D., Griffiths, M.J., Granerod, J., Brown, D., Keir, G., Wnęk, G., Cox, D.J., Vidyasagar, R., Borrow, R., Parkes, L.M., and Solomon, T. (2016b). The Interleukin-1 Balance During Encephalitis Is Associated With Clinical Severity, Blood-Brain Barrier Permeability, Neuroimaging Changes, and Disease Outcome. J. Infect. Dis. 213, 1651–1660.

Miyabe, Y., Miyabe, C., Murooka, T.T., Kim, E.Y., Newton, G.A., Kim, N.D., Haribabu, B., Luscinskas, F.W., Mempel, T.R., and Luster, A.D. (2017). Complement C5a receptor is the key initiator of neutrophil adhesion igniting immune complex-induced arthritis. Sci. Immunol. 2, eaaj2195.

Miyabe, Y., Miyabe, C., Mani, V., Mempel, T.R., and Luster, A.D. (2019). Atypical complement receptor C5aR2 transports C5a to initiate neutrophil adhesion and inflammation. Sci. Immunol. 4, eaav5951.

Phillipson, M., Heit, B., Parsons, S.A., Petri, B., Mullaly, S.C., Colarusso, P., Gower, R.M., Neely, G., Simon, S.I., and Kubes, P. (2009). Vav1 is essential

for mechanotactic crawling and migration of neutrophils out of the inflamed microvasculature. J. Immunol. *182*, 6870–6878.

Pineau, I., Sun, L., Bastien, D., and Lacroix, S. (2010). Astrocytes initiate inflammation in the injured mouse spinal cord by promoting the entry of neutrophils and inflammatory monocytes in an IL-1 receptor/MyD88-dependent fashion. Brain Behav. Immun. *24*, 540–553.

Piret, J., and Boivin, G. (2015). Innate immune response during herpes simplex virus encephalitis and development of immunomodulatory strategies. Rev. Med. Virol. *25*, 300–319.

Roy, M., Richard, J.F., Dumas, A., and Vallières, L. (2012). CXCL1 can be regulated by IL-6 and promotes granulocyte adhesion to brain capillaries during bacterial toxin exposure and encephalomyelitis. J. Neuroinflammation *9*, 18.

Rubio, N., and Sanz-Rodriguez, F. (2007). Induction of the CXCL1 (KC) chemokine in mouse astrocytes by infection with the murine encephalomyelitis virus of Theiler. Virology *358*, 98–108.

Rueden, Curtis, T, Schindelin, Johannes, Hiner, Mark, C, DeZonia, Barry, E, Walter, Alison, E, Arena, Ellen, T, and Eliceiri, Kevin, W. (2017). ImageJ2: ImageJ for the next generation of scientific image data. BMC Bioinformatics *18*, 529.

Saederup, N., Cardona, A.E., Croft, K., Mizutani, M., Cotleur, A.C., Tsou, C.L., Ransohoff, R.M., and Charo, I.F. (2010). Selective chemokine receptor usage by central nervous system myeloid cells in CCR2-red fluorescent protein knock-in mice. PLoS ONE *5*, e13693.

Semple, B.D., Kossmann, T., and Morganti-Kossmann, M.C. (2010). Role of chemokines in CNS health and pathology: a focus on the CCL2/CCR2 and CXCL8/CXCR2 networks. J. Cereb. Blood Flow Metab. *30*, 459–473.

Sergerie, Y., Rivest, S., and Boivin, G. (2007). Tumor necrosis factor-alpha and interleukin-1 beta play a critical role in the resistance against lethal herpes simplex virus encephalitis. J. Infect. Dis. *196*, 853–860.

Shen, F., Jiang, L., Han, F., Degos, V., Chen, S., and Su, H. (2019). Increased Inflammatory Response in Old Mice is Associated with More Severe Neuronal Injury at the Acute Stage of Ischemic Stroke. Aging Dis. *10*, 12–22.

Si, Y., Tsou, C.L., Croft, K., and Charo, I.F. (2010). CCR2 mediates hematopoietic stem and progenitor cell trafficking to sites of inflammation in mice. J. Clin. Invest. *120*, 1192–1203.

Smith, G.A., Gross, S.P., and Enquist, L.W. (2001). Herpesviruses use bidirectional fast-axonal transport to spread in sensory neurons. Proc. Natl. Acad. Sci. USA *98*, 3466–3470.

Smith, C.J., Hulme, S., Vail, A., Heal, C., Parry-Jones, A.R., Scarth, S., Hopkins, K., Hoadley, M., Allan, S.M., Rothwell, N.J., et al. (2018). SCIL-STROKE (Subcutaneous Interleukin-1 Receptor Antagonist in Ischemic Stroke): A Randomized Controlled Phase 2 Trial. Stroke *49*, 1210–1216.

Soehnlein, O., Steffens, S., Hidalgo, A., and Weber, C. (2017). Neutrophils as protagonists and targets in chronic inflammation. Nat. Rev. Immunol. *17*, 248–261.

Solomon, T., Michael, B.D., Smith, P.E., Sanderson, F., Davies, N.W.S., Hart, I.J., Holland, M., Easton, A., Buckley, C., Kneen, R., and Beeching, N.J.; National Encephalitis Guidelines Development and Stakeholder Groups (2012). Management of suspected viral encephalitis in adults—Association of British Neurologists and British Infection Association National Guidelines. J. Infect. *64*, 347–373.

Tani, M., Fuentes, M.E., Peterson, J.W., Trapp, B.D., Durham, S.K., Loy, J.K., Bravo, R., Ransohoff, R.M., and Lira, S.A. (1996). Neutrophil infiltration, glial reaction, and neurological disease in transgenic mice expressing the chemokine N51/KC in oligodendrocytes. J. Clin. Invest. *98*, 529–539.

Teixeira, M.M., Vilela, M.C., Soriani, F.M., Rodrigues, D.H., and Teixeira, A.L. (2010). Using intravital microscopy to study the role of chemokines during infection and inflammation in the central nervous system. J. Neuroimmunol. *224*, 62–65.

Thomas, H.C., Kapadia, R.D., Wells, G.I., Gresham, A.M., Sutton, D., Solleveld, H.A., Sarkar, S.K., Dillon, S.B., and Tal-Singer, R. (2001). Differences in pathogenicity of herpes simplex virus serotypes 1 and 2 may be observed by histopathology and high-resolution magnetic resonance imaging in a murine encephalitis model. J. Neurovirol. *7*, 105–116.

Venkatesan, A., Michael, B.D., Probasco, J.C., Geocadin, R.G., and Solomon, T. (2019). Acute encephalitis in immunocompetent adults. Lancet *393*, 702–716.

Vilela, M.C., Mansur, D.S., Lacerda-Queiroz, N., Rodrigues, D.H., Arantes, R.M., Kroon, E.G., Campos, M.A., Teixeira, M.M., and Teixeira, A.L. (2008). Traffic of leukocytes in the central nervous system is associated with chemokine up-regulation in a severe model of herpes simplex encephalitis: an intravital microscopy study. Neurosci. Lett. *445*, 18–22.

Vilela, M.C., Lima, G.K., Rodrigues, D.H., Lacerda-Queiroz, N., Mansur, D.S., de Miranda, A.S., Rachid, M.A., Kroon, E.G., Vieira, L.Q., Campos, M.A., et al. (2010). TNFR1 plays a critical role in the control of severe HSV-1 encephalitis. Neurosci. Lett. *479*, 58–62.

Vilela, M.C., Lima, G.K., Rodrigues, D.H., Lacerda-Queiroz, N., Pedroso, V.S.P., Miranda, A.S., Rachid, M.A., Kroon, E.G., Campos, M.A., Teixeira, M.M., et al. (2013). Absence of CCR5 increases neutrophil recruitment in severe herpetic encephalitis. BMC Neurosci. *14*, 19.

Voisin, M.B., Leoni, G., Woodfin, A., Loumagne, L., Patel, N.S., Di Paola, R., Cuzzocrea, S., Thiemermann, C., Perretti, M., and Nourshargh, S. (2019). Neutrophil elastase plays a non-redundant role in remodeling the venular basement membrane and neutrophil diapedesis post-ischemia/reperfusion injury. J. Pathol. *248*, 88–102.

Wang, P., Bai, F., Zenewicz, L.A., Dai, J., Gate, D., Cheng, G., Yang, L., Qian, F., Yuan, X., Montgomery, R.R., et al. (2012). IL-22 signaling contributes to West Nile encephalitis pathogenesis. PLoS ONE *7*, e44153.

Weninger, W., Biro, M., and Jain, R. (2014). Leukocyte migration in the interstitial space of non-lymphoid organs. Nat. Rev. Immunol. *14*, 232–246.

West, D.M., Del Rosso, C.R., Yin, X.T., and Stuart, P.M. (2014). CXCL1 but not IL-6 is required for recurrent herpetic stromal keratitis. J. Immunol. *192*, 1762–1767.

Wuest, T.R., and Carr, D.J.J. (2008). The role of chemokines during herpes simplex virus-1 infection. Front. Biosci. *13*, 4862–4872.

Zhou, J., Stohlman, S.A., Hinton, D.R., and Marten, N.W. (2003). Neutrophils promote mononuclear cell infiltration during viral-induced encephalitis. J. Immunol. *170*, 3331–3336.

STAR★METHODS

KEY RESOURCES TABLE

REAGENT or RESOURCE	SOURCE	IDENTIFIER
Antibodies		
TruStain fcX anti-mouse CD16/32 (Clone 93)	Biolegend	Cat# 101320, RIID:AB_1574973
APC-conjugated CD45 (Clone 30-F11)	Biolegend	Cat#103112, RRID:AB_312977
PE-conjugated CD11b (Clone M1/70)	Biolegend	Cat# 101208, RRID:AB_312791
BV605-conjugated CD11c (Clone N418)	Biolegend	Cat# 117334, RRID:AB_2562415
BV421-conjugated Ly6G (Clone 1A8)	BD Biosciences	Cat# 562737, RRID:AB_2737756
FITC-conjugated Ly6C (Clone AL-21)	BD Biosciences	Cat# 553104, RRID:AB_394628
AF647-conjugated CD31 (Clone 390)	Biolegend	Cat# 102415, RRID:AB_493411
PE-conjugated CD31 (Clone 390)	Biolegend	Cat# 102408, RRID:AB_312903
APC-conjugated Ly6G (Clone 1A8)	Biolegend	Cat# 127613, RRID:AB_1877163
eFluor 780-conjugated viability dye	ThermoFisher Scientific	Cat# 65-0865-14
rabbit polyclonal anti-CXCL1-AF555	Bioss	Cat# bs-10234R-AF555
rabbit polyclonal IgG2b isotype control	Bioss	Cat# bs-0295P-AF555
FITC-conjugated NeuN	Abcam	Cat# ab223994
Pacific Blue-conjugated CD11b (Clone M1/70)	Biolegend	Cat# 101223, RRID:AB_755985
APC-conjugated GFAP (Clone S206A-8)	Sigma	Cat# SAB5201114, RRID:AB_2827276
Albumin–fluorescein isothiocyanate conjugate (FITC-Albumin)	Sigma	Cat# A9771
InVivoMab anti-mouse Ly6G (Clone 1A8)	Bxcell	Cat# BE0075-1, RRID:AB_1107721
InVivoMab rat IgG2a isotype control (Clone 2A3)	Bxcell	Cat# BE0089, RRID:AB_1107769
Bacterial and Virus Strains		
HSV-1-KOS	David Knipe (Harvard Medical School)	Colgrove et al., 2016
VP26-eGFP-HSV-1	David Knipe (Harvard Medical School)	Desai et al., 1998
Chemicals, Peptides, and Recombinant Proteins		
Phosphate-Buffered Saline	Sigma	Cat# P-4417
Acyclovir	Tocris	Cat# 2513/50
Evans Blue	Sigma	Cat# E2129-10G
Xylazine	Patterson Veterinary	Cat# 78081939
Ketamine	Patterson Veterinary	Cat# 78908590
Triton X-100	Sigma	Cat# 11332481001
IL1RA, Kineret (Anakinra)	Sobi, Inc	
Fetal Bovine Serum	Sigma	Cat# F2442
L-Glutamine	Sigma	Cat# G7513
Glutamax	Fisher Scientific	Cat# 35-050-061
HEPES	Corning	Cat# 25-060-CI
Penicillin/Streptomycin	Lonza	Cat# 17-602E
IgG Human Serum	Sigma	Cat# I4506, RRID:AB_1163606
Percoll	GE Life Sciences	Cat# 17089102
Serum-Free Protein Block	Agilent	Cat# X090930-2
Antibody diluent	Agilent	Cat# S080981-2
ProLong™ Diamond Antifade Mountant with DAPI	Thermo Fisher Scientific	Cat# P36962
ProLong™ Diamond Antifade Mountant	Thermo Fisher Scientific	Cat# P36961
UltraComp eBeads	eBioscience	Cat# 01-2222-41
CountBright™ counting beads	Thermo Fisher Scientific	Cat# C36950

(Continued on next page)

Continued

REAGENT or RESOURCE	SOURCE	IDENTIFIER
Xylocaine 2%	AAP Pharmaceuticals	Cat# 43323049231
Qdot-605	Thermo Fisher Scientific	Cat# Q25021MP
MultiScribe Reverse Transcriptase	Thermo Fisher Scientific	Cat# 4311235
TRIzol™ Reagent	Thermo Fisher Scientific	Cat# 15596026
Critical Commercial Assays		
Cytometric Bead Array	EMD Millpore	Cat# MCYTMAG-70K-PX32
Mouse Albumin ELISA Kit	Abcam	Cat# ab108791
QuantiFast SYBR Green RT-PCR Kit (400)	Qiagen	Cat # 204154
Primary Neurons from CD1 mice	ScienCell Research	Cat# M1520
Microglia from CD1 mice	ScienCell Research	Cat# M1900
Astrocytes from CD1 mice	ScienCell Research	Cat# M1820
Poly-L-Lysine, 1 mg/ml	ScienCell Research	Cat# 0403
Neuronal medium	ScienCell Research	Cat# 1521
Microglia medium	ScienCell Research	Cat# 1901
Astrocyte medium	ScienCell Research	Cat# 1831
Vero cells	Thorsten Mempel (Massachusetts General Hospital)	
DMEM	Corning	Cat# 15-013-CV
Experimental Models: Organisms/Strains		
Mouse: C57BL/6	Charles River Laboratories	Cat# 556
Mouse: C57BL/6-CCR2$^{-/-}$	Jackson Laboratory	Cat# 17586
Mouse: C57BL/6-CXCR2$^{-/-}$	Jackson Laboratory	Cat# 6848
Mouse: C57BL/6-LysM-GFP	Thomas Graf (Albert Einstein College of Medicine)	Faust et al., 2000
Mouse: C57BL/6-CCR2-RFP/CX3CR1-GFP	Joseph El Khoury (Massachusetts General Hospital)	Parent strains 005582 and 017586, Saederup et al., 2010
Oligonucleotides		
IL-1α Forward: 5'-TCTATGATGCAAGCTATGG CTCA-3'	Integrated DNA Technologies	
IL-1α Reverse: 5'-CGGCTCTCCTTGAAGGTGA-3'	Integrated DNA Technologies	
Software and Algorithms		
FlowJo	TreeStar Inc.	V10.6.1
Zen	Zeiss	Oberkochen, Germany
Prism 8	Graphpad	N/A
ImageJ	National Institutes of Health (NIH)	Rueden et al., 2017
Imaris	Bitplane	

RESOURCE AVAILABILITY

Lead contact
Further information and requests for resources and reagents should be directed to and will be fulfilled by the Lead Contact, Andrew D Luster (aluster@mgh.harvard.edu).

Materials availability
This study did not generate new unique reagents.

Data and code availability
This study did not generate/analyze datasets or code.

EXPERIMENTAL MODEL AND SUBJECT DETAILS

HSV strains

HSV-1-KOS (Colgrove et al., 2016) and VP26-eGFP-HSV-1 (Desai et al., 1998) were kindly provided by D.M. Knipe (Harvard Medical School) and prepared and titrated using Vero cells grown in Dulbecco's modified Eagle's medium (DMEM) supplemented with 10% fetal calf serum, 1% HEPES, 1% GlutaMAX, penicillin G, and streptomycin (Brockman and Knipe, 2002).

Mice and infection model

Approval for the study was obtained from the Partners Healthcare Institutional Animal Care and Use Committee. C57BL/6 female mice were obtained from Charles River Laboratories. $Ccr2^{-/-}$ (Si et al., 2010), $Cxcr2^{-/-}$ (Cacalano et al., 1994) and LysM-GFP mice (Faust et al., 2000) in the C57BL/6 background were maintained in our mouse colony. $Cxcr2^{-/-}$LysM-GFP were generated in house by breeding $Cxcr2^{-/-}$ and LysM-GFP mice. CCR2-RFP/CX3CR1-GFP mice (Saederup et al., 2010) were kindly supplied by J. El Khoury (Massachusetts General Hospital). Mice used for the experiments were females aged 8-14 weeks. Mice were aged 12-14 weeks for intravital microscopy studies to ensure sufficiently robust ossification of cranial sutures thereby limiting cerebral trauma during craniotomy surgery. Mice were anaesthetized with isoflurane and underwent intracranial infection using a Teflon-depth-restricted fine-bore needle (BD Biosciences and Sigma Aldrich), through the sagittal suture with either 20uL of HSV-KOS $1\times10^{4-5}$ in PBS or sham infection with sterile PBS into the subarachnoid space (Kurt-Jones et al., 2004). Acyclovir (Tocris) was reconstituted in sterile PBS and injected intraperitoneally (50mg/kg) daily commencing 24hours after i.c. infection. Acyclovir was administered in all the experiments using $Ccr2^{-/-}$ and $Cxcr2^{-/-}$ mice in order to reflect clinical disease management in humans.

Primary cell cultures

Primary neurons, microglia, and astrocytes isolated from CD1 mice were obtained from ScienCell Research Laboratories (Carlsbad, CA). Neurons and microglia were seeded onto 24 well cell culture plates coated with Poly-L-Lysine (10 μg/ml) (ScienCell Research Laboratories), while astrocytes were first expanded in a Poly-L-Lysine coated T-75 flask prior to seeding onto Poly-L-Lysine coated 24 well cell culture plates. Neurons, microglia and astrocytes were maintained in neuronal medium, microglia medium, and animal astrocyte medium (ScienCell Research Laboratories) respectively, until confluent and ready to use.

Cell lines

Vero cells were provided by Thorsten Mempel (Massachusetts General Hospital). The cells were maintained and sub-cultured in Dulbecco's modified Eagle's medium (DMEM) supplemented with 10% fetal calf serum, 1% HEPES, 1% GlutaMAX, penicillin G, and streptomycin (Brockman and Knipe, 2002).

METHOD DETAILS

Neurological Disease Severity score and Evans Blue assessment of BBB permeability

Following infection mice were examined twice daily using an established score of murine neurological morbidity due to HSV-1 encephalitis (Thomas et al., 2001). To visualize BBB permeability, mice were anaesthetized with ketamine/xylazine and injected intravenously with 100ul of 2% Evans blue in sterile PBS 30 min prior to euthanasia following a modified version of previously established methodology (Bennett et al., 2010; Shen et al., 2019). Mice were then euthanized with CO_2 and death confirmed by transection of the great arteries. A craniotomy was performed and images taken. For the assessment of BBB permeability using the brain to serum albumin ratio, a cardiac puncture was performed to extract blood immediately after euthanasia performed with CO_2. The blood was left to clot for 30 min at 4°C and centrifuged at 5,000 rpm for 5 min to obtain serum. A craniotomy was performed and brains were homogenized in PBS using a BeadBeater (Biospec) followed by a centrifugation at 15,000 rpm for 5 min. The levels of albumin in serum and brain was assessed by performing an ELISA on the serum and brain supernatants following the manufacturer's instructions (Cat ab108791, Abcam).

Flow cytometry

Leukocytes were isolated from brain samples which were dissociated using GentleMACS and isolated on a discontinuous 70:30 Percoll gradient (Gelifesciences). The meninges were not removed from the brain, therefore the leukocyte populations identified reflect those of the parenchyma and cerebral meninges. Cells were blocked with TruStain fcX anti-mouse CD16/32 antibody (Biolegend, Clone 93, Cat# 101320, 1:25) and stained with the following primary antibodies: APC-conjugated CD45 antibody (Biolegend, Clone 30-F11, Cat#103112, 1:400), PE-conjugated CD11b antibody (Biolegend, Clone M1/70, Cat# 101208, 1:200), BV605-conjugated CD11c antibody (Biolegend, Clone N418, Cat# 117334, 1:400), BV421-conjugated Ly6G antibody (BD Biosciences, Clone 1A8, Cat# 562737, 1:200) and the FITC-conjugated Ly6C antibody (Biolegend, Clone AL-21, Cat# 553104, 1:200).

UltraComp eBeads (eBioscience) were used for compensation and heat-shocked spleenocytes for viability control using eFluor 780-conjugated viability dye (eBioscience). Samples were analyzed on a LSRII (BD Bioscience) with fluorescent CountBright™ counting beads (Thermofisher). All data analysis was performed using the flow cytometry analysis program FlowJo (Treestar).

Luminex bead-based multiplex assay

Whole brains were isolated into 1mL sterile PBS and homogenized with 1mm glass beads using a BeadBeater (Biospec). The solution was centrifuged at 15,000 rpm for 5 min and the supernatant collected. Prior to analysis, the supernatants were incubated for 1h at room temperature with 10% Triton X-100 at a ratio of 20:1 to inactivate the viral particles. Levels of the following 32 cytokines and chemokines were assessed using a Luminex bead-based multiplex assay (MCYTMAG-70K-PX32, EMD Millipore): G-CSF, GM-CSF, M-CSF, TNF-α, IFN-γ, IL-1α, IL-1β, IL-2, IL-3, IL-4, IL-5, IL-6, IL-7, IL-9, IL-10, IL-12 (p40), IL-12 (p70), IL-13, IL-15, IL-17, CXCL1, CXCL2, CXCL5, CXCL9, CXCL10, LIF, CCL2, CCL3, CCL4, CCL5, CCL11, and VEGF. IL-1RA (Kineret ®) 10mg/kg or dexamethasone (Sigma) 8mg/kg was given i.p. immediately following infection.

Plaque assay

Vero cells were seeded on 24 well plates at a concentration of 2.2×10^5 cells/ml. When 90% confluency was reached, the cells were incubated for 1h with serially diluted brain homogenate supernatant, isolated as above for the Luminex assay, in serum free DMEM medium at $37°C$. The virus was removed by washing the cells with sterile PBS and 1ml of DMEM medium supplemented with FBS, Pen/strep, L-Glutamine, and human IgG (Sigma Aldrich) was added and the cells were incubated at $37°C$ for 48h (Kurt-Jones et al., 2004). The infected cells were then fixed and stained with crystal violet, and PFUs were calculated by counting the plaques in the dilution well containing 10-100 plaques.

Confocal microscopy

Euthanasia was performed with CO_2. A post-mortem craniotomy was performed and the whole brain carefully resected, fixed in PLP for 12 h, then dehydrated using serial sucrose-gradient osmosis. Brains were then embedded in OCT, frozen in 3,4 Methyl Butane, and stored at $-80°C$. 12 μm sections of organotypic tissue were cut using a crytostat, mounted on glass slides, and blocked for 10 min with serum-free Dako block (Agilent). To study CXCL1 co-localization sections were stained with the following antibodies prepared in antibody dilutent (# S080981-2 Agilent) in addition to mounting media (# P36970 Thermofisher): rabbit polyclonal anti-CXCL1-AF555 (# 10234R Bioss 1:100) or rabbit polyclonal IgG2b isotype control (#0295P Bioss 1:100), GFAP-APC (# SAB5201114 Sigma 1:100), NeuN-FITC (#ab223994 Abcam 1:100) and CD11b-Pacific Blue (#101223 Biolegend 1:100). To study localization of neutrophils in CCR2-RFP/CX3CR1-GFP infected mice sections were stained with the following antibodies prepared in antibody dilutent including DAPI nuclear stain (# P36962 Thermofisher): Ly6G-BV421 (# 562737 Biolegend) and CD31-AF647 (# 102415 Biolegend). For the FITC-albumin experiments, mice were anaesthetized with ketamine/xylazine and injected iv with 10 mg of FITC albumin 60 min prior to euthanasia. Stained sections were imaged with unstained and isotype controls using a Zeiss Confocal Microscope (Zeiss, Oberkochen, Germany). FITC albumin was quantitated by determining the FITC fluorescence across organotypic brain tissue slices relative to DAPI nuclear signal to adjust for cell count between samples using ImageJ software (Rueden et al., 2017).

Wide-field microscopy

Cerebral cortex was dissected from underlying deep white matter, corpus callosum, caudate, and brain stem on DPI 1 into 3mm sections and placed into PAB (PBS, 1% BSA, and 0.1% sodium azide) on ice. Samples were blocked with Trustain FcX (anti-mouse CD16/32; Biolegend 10 μg/mL) and incubated with antibodies for 2 hr at $4°C$: PE-conjugated anti-CD31 (#102408 Biolegend 8 μL), APC-conjugated anti-CD45 (#103112 clone 30-F11 Biolegend 5 μL) or APC-conjugated anti-Ly6G (#127613 Biolegend 5 μL). Samples of stained cortex were then washed in PAB, placed on a microscope slide and imaged using a wide-field fluorescence microscope and monochrome CCD digital camera and analyzed using Zen Blue software (Zeiss, Oberkochen, Germany).

In vitro infection of primary cells

Primary neurons (#M1520), microglia (#M1900) and astrocytes (#M1820) isolated from CD1 mice where purchased from ScienCell Research Laboratories (Carlsbad, CA). Cells were cultured in 24 well plates; neurons were seeded at a density of 8.3×10^4 cells/well, while astrocytes and microglia were seeded at a density of 3×10^4 cell/well. Once cells were confluent they were infected with HSV-1 KOS at a multiplicity of infection (MOI) of 0.1, 1 and 10 for 1h. Following incubation with the virus the cells were washed twice with PBS and incubated with the appropriate media for an additional 24h. After incubation the supernatant was collected and stored at $-80°C$ for analysis of cytokine and chemokine secretion using the Luminex multiplex assay described above.

Cranial window surgery and multi-photon intravital microscopy

Mice 4-6 hr post-infection were anesthetized by i.p. injection of Ketamine/Xylazine and positioned on a custom stereotactic surgical stage on a $37°C$ heating pad, and the skull immobilized. Hair in the frontal and parietal regions of the skull was removed using #40 electrical hair clippers and a chemical depilatory agent (Nair). To reduce the risk of wound infections, the skin was cleaned with an ethyl alcohol solution and surgery performed under aseptic conditions. A bolus of 100uL of 2% Xylocaine (AAP Pharmaceuticals, LLC) was injected subcutaneously over the vertex of the cranium. After 2–3 min a semicircle of skin was excised from the top of the skull, and the underlying periosteum scraped off. Using a high-speed air-turbine drill with a burr tip size of 0.8 mm in diameter (Fine Science Tools), a groove was made to form a circle of approximately 4mm in the parietal bone of the skull. This area was made thinner by cautious and continuous drilling of the groove until the bone flap became loose. Cold sterile PBS was applied during

the drilling process to avoid thermal injury of the cortical regions of the CNS. Using a blunt microblade, the bone flap was separated from the dura mater underneath, leaving the dura intact. After removal of the bone flap, the dura mater was continuously kept moist with physiological saline. The window was then sealed by adhering a 5mm cover glass to the bone using a histocompatible cyano-acrylate tissue glue (Elmer's Products LLC) and powdered dental repair powder (Lang Dental Manufacturing Co. Inc). The mouse was then injected intravenously with a 5 μL Qdots 605® in 100 μL PBS and placed on custom-built microscopy platform for imaging, while still under anesthesia. Immersol W 2010 immersion medium was placed between the cranial window and the 20x lens, and window temperature maintained with an objective warmer (Warner).

MP-IVM was performed using Spectra-Physics Insight DS (830) and MaiTai BB (920) lasers on an Olympus MPE-RS microscope using Olympus FV305-SW acquisition software. The post-capillary venules of the right parietal cortex of mice were imaged over 23 mins with 4 μm optical sections sequentially scanned over 11 z stacks with 1x optical zoom and a 20x lens providing image volumes of 40 μm depth and 512 μm width. Rendered movies were analyzed with Imaris© (Bitplane). To determine the vessel surface the QTracker-605® signal was determined at baseline and a surface computed with Imaris©; *LysM*-GFP cells identified outside of this surface were analyzed reflecting extravasated neutrophils and *LysM*-GFP cells identified within this surface were analyzed reflecting intravascular neutrophils. The migratory behavior of *LsyM*-GFP cells was determined and neutrophils were defined as slow rolling, crawling, or arrested if they exhibited a speed of 10-40, 2-10 or < 2 μm/sec, respectively, as previously determined (Phillipson et al., 2009). Blood brain barrier permeability was quantified as volume of QTraquer-605® observed outside of the vessel surface. The data obtained from the multi-photon intravital microscopy were determined by combining data from 3 independent experiments.

Reverse Transcription Quantitative PCR (RT-qPCR)
Total RNA was collected from primary cell cultures using TRIzol reagent (ThermoFisher) according to manufacturer's protocol, diluted in RNase-free water, and stored at −80°C. cDNA was prepared using reverse transcription, and gene expression quantitated using a Roche Lightcycler 96 Real-Time PCR system and SYBR Green Master Mix (Roche). Values were calculated relative to Gapdh. Validated primer pairs were selected from the MGH PrimerBank.

Mouse Primers
IL-1α Forward: 5′-TCTATGATGCAAGCTATGGCTCA-3′; IL-1α Reverse: 5′-CGGCTCTCCTTGAAGGTGA-3′.

Neutrophil depletion
Neutrophils were depleted 24h prior to infection and on days 1 and 3 post-infection by injecting i.p. 0.5 mg of anti-mouse Ly6G antibody or isotype control (Bxcell).

QUANTIFICATION AND STATISTICAL ANALYSES

Mice were randomly assigned to receive i.c. HSV-1 or PBS injection, and to receive i.p. acyclovir or PBS. For flow cytometric studies, a sample size of 6 mice/group provided a 90% power to show a mean difference of 1.5 standard deviation (SD) between the groups (based on a two-sample t test with a 2-sided 5% significance level). Significance testing was performed between two groups by Student's t test when data were normally distributed and when data were not by Wilcoxon rank sum test, and Fisher's exact test were appropriate. We used a two-way ANOVA for multiple group data when data were normally distributed and Linear regression for correlation analyses. Sample sizes and statistical information can be found in the figure legends. Data were analyzed using GraphPad PRISM (2018).